FOURTH SEMI-ANNUAL TECHNICAL REPORT

ELECTRICAL and OPTICAL PROPERTIES of AMORPHOUS MATERIALS*

by

A Solid-State Group of the Physics Department
Northern Illinois University
DeKalb, Illinois 60115

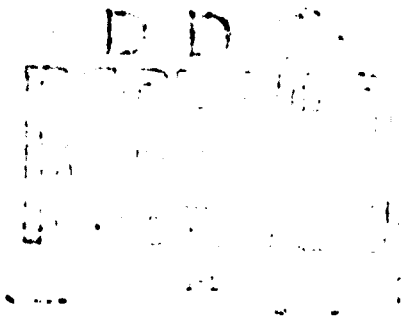

*Sponsored by
Advanced Research Projects Agency
ARPA Order No. 1562

GENERAL INFORMATION

ARPA Order Number	1562
Program Code Number	0D10
Name of Contractor	U. S. Army Research Office
Effective Date of Contract	June 1, 1971
Contract Expiration Date	May 31, 1972
Amount of Contract	$58,000.00
Contract Number	DA-ARO-D-31-124-71-G132
Principal Investigator	Dr. Charles Wood (815) 753-1773

CONTENTS

SUMMARY

During the last six months much of the work reported in preliminary form in the last semi-annual report has been completed.

In this summary some of the highlights of finished work as well as research in progress will be mentioned.

The electronic structure of Sb_2Se_3, both crystalline and amorphous, has been studied in much detail, and the combination of four types of spectroscopy (optical reflectivity, photoemission, photoconductivity, and ESCA) has led to a reasonably complete picture of the electronic structure. This picture has further implications regarding the bonding in this compound in its crystalline and amorphous states. This work is synopsized in the body of the report and preprints to be submitted for publication detailing the various measurements and their interpretation are attached to the report.

Resistivity vs. temperature measurements have been made on crystalline and amorphous Sb_2Se_3 in order to ascertain the "thermal" energy gap in these materials. A reproducible variation of the gap in crystalline Sb_2Se_3 attributable to small compositional variations was found. This work is outlined in the report.

A new and improved evaporation system is being constructed in order to eliminate the problems in controlling the rates of evaporation in the double-source film preparation system. This is necessary in order to maintain the strictest possible control on the homogeneity of the resultant film. This work is discussed as are some preliminary results upon the mass density of evaporated amorphous Sb_2Se_3 films.

Differential thermal analysis measurements are continuing on thin amorphous films of Sb_2Se_3 in order to determine, if possible, their glass transition temperature. A preliminary report of this research is also presented.

Measurements (photoconductivity, photoemission, optical transmission and reflectivity) have been initiated on Sb_2Te_3 (crystalline and amorphous) and preliminary optical studies have been made on Sb_2O_3. Research in progress on these compounds is discussed in Sec. III.

Finally Mossbauer spectroscopy is being initiated on amorphous Sb, Sb_2Te_3, and Sb_2S_3 (both crystalline and amorphous) in order to obtain information about the chemical and electronic structure of the amorphous state of these materials. Sec. IV describes the initial phases of this research, and also outlines the continuing X-ray and electron diffraction studies on V-VI materials.

In addition to the preprints on the electronic structure of Sb_2Se_3 (Appendices A, B and C) further appendices include a preprint describing the optical studies and preparation of Sb_2O_3 (Appendix D) and three abstracts of papers presented at the March meeting of the American Physical Society (Appendix E).

I. THEORETICAL RESEARCH

A) Kramers-Kronig Analysis

The Kramers-Kronig method we developed [1] has been applied to Sb_2Se_3 successfully (see Appendix A). Several improvements in the program have greatly increased its speed and now a complete analysis of reflectivity data can be accomplished in about 1 minute of CPU time on the 360/67 computer. The reflectivity data employed are on a constant energy mesh of 0.1 eV from 0 → 25 eV and thus 251 data points are involved. Presently the program is being streamlined in order to decrease the storage required so that it can be run on smaller machines and/or a finer mesh in the data can be used. In addition we are applying the analysis in a preliminary fashion to reflectivity data on p-type (degenerate) Sb_2Te_3 as part of the preparation for a thorough study of this compound in its crystalline and amorphous modifications.

B) Electronic Structure

The electronic structure of Sb_2Se_3 is, of course, of much interest to us since we have available a wealth of experimental information (see Sec. II below). The large, orthorhombic unit cell containing 28 atoms makes a band calculation quite formidable as mentioned in the last semi-annual report. Thus it seems that a calculation only at high symmetry points and lines in the Brillouin zone would be an economical test. Therefore we are continuing to compute the band structure of Sb_2Se_3 by pseudopotential means restricting ourselves at least initially to symmetry

points and thus using rather small basis sets. Approximate densities of states and optical characteristics will be derived from the results and the utility of a more complete and general calculation assessed.

Investigation of the possibility of using an almost periodic pseudopotential to approximate the electronic structure of a solid with short-range but not long-range order is in progress. An almost periodic pseudopotential can be written

$$V(\underline{r}) = \sum_{\underline{K}} V(\underline{K})\ e^{i\underline{K}\cdot\underline{r}},$$

in which the $\underline{K}$'s are a discrete set of vectors in reciprocal space not necessarily on a lattice. Thus, if we could choose a suitable set of $\underline{K}$'s, we could deal with a problem formally similar to the periodic pseudopotential problem but capable, in principle, of dealing with the loss of long-range order as pointed out by Romerio [2]. Work continues as to how to appropriately select the $\underline{K}$'s and how to efficiently solve the secular equation for the pseudo-Schrodinger equation with such a pseudopotential.

RESEARCH ON Sb_2Se_3

A) Spectroscopic Studies of Electron State of Crystalline and Amorphous Sb_2Se_3

1) Introduction

The electronic structure of crystalline and amorphous Sb_2Se_3 has been of great interest throughout our work [3]. Because the crystal is highly anisotropic and has an extremely complex unit cell (28 atoms, 112 valence electrons) a band structure calculation is very difficult. However a judicious combination of experimental data and analysis (optical reflectivity with Kramers-Kronig transformation, photoemission, and ESCA measurements) coupled with a simple chemical bonding model allows the development of a rather complete semi-empirical picture of the density of electronic states in this material. The model includes a tentative explanation of some differences between the amorphous and crystalline materials. Furthermore because of its general character it may be applicable to several V-VI compounds.

The details of the model are presented in Appendices A, B and C. Appendix A is a rather major revision of Appendix A of the previous semi-annual report and is included here for the purpose of making this report self-contained. Appendix B presents the photoemission results and Appendix C the ESCA data. Both Appendix B and C give detailed comparisons with the optical results.

The principle component of the model is the division of the valence electrons into weakly bonding resonance states and covalent bonding states, which division accounts for most of the valence band structure. Structure

occurring in the conduction band density of states can be inferred on the basis of the ESCA and photoemission results as well as effects which depend upon matrix elements and introduce anisotropy in the crystal. Alternative explanations of the lower $\varepsilon_2(h\nu)$ values for the amorphous material relative to the crystal in the visible and near ultraviolet are advanced.

2) Reflectivity and Other Optical Measurements

The reflectivity of crystalline and amorphous Sb_2Se_3 has been measured and Kramers-Kronig analyzed in order to characterize the effect of the transition from the crystalline to amorphous state upon the electronic states in this compound. A preliminary version of this work was included in the last semi-annual report. A more polished and complete preprint detailing that research is appended (Appendix A) to this report. The Kramers-Kronig analysis has been improved principally by increasing the precision of the extrapolations of the reflectivity. In addition the accuracy of the numerical procedures has been optimized, i.e., the error in the Kramers-Kronig data inversion, has been made minimal. A much more detailed interpretation of the results has been made based upon the valence bonding model of Sb_2Se_3 of Mooser and Pearson [4] and the structural work on the compound of Tideswell, et. al. [5].

Several attempts were made to measure the static dielectric constant of crystalline Sb_2Se_3 at liquid nitrogen temperature. The results, which exhibited considerable variation, ranged between 13 and 17.

A sample of Sb_2Se_3 has been cleaved to a thickness of 338 $\mathring{A}$. Optical measurements at energies greater than the fundamental edge on this sample

indicate the onset of a strong direct absorption process for a photon energy of about 2.4 eV for both polarizations of light in the cleavage plane. The reflectivity for the polarization perpendicular to the cleavage plane is being taken on a cut, polished and etched sample using a technique developed by Veal [6]. Transmission and reflectivity measurements in the region of the fundamental absorption edge (and their analysis) in order to determine the indirect and direct absorption thresholds in Sb_2Se_3 are in progress.

3) Photoemission

Important results related closely to the electronic structure of crystalline and amorphous Sb_2Se_3 were obtained from photoemission spectra in the photon energy region 7 eV to 35 eV. The results were obtained using the synchrotron storage ring at the University of Wisconsin. The main features of our photoemission spectra are: 1) a strong effect of $\vec{k}$ conservation and of matrix elements in the case of crystalline Sb_2Se_3 as demonstrated by direct transitions which have polarization dependent strength (polarization of exciting radiation is essential for this experiment), 2) waiving of the $\vec{k}$ conservation in case of amorphous Sb_2Se_3 as demonstrated by non-direct transitions. 3) a high density of states in the conduction band at the region 7 eV to 10 eV above the top of the valence band for both crystalline and amorphous Sb_2Se_3, which is further confirmed by the ESCA spectrum, 4) it is the region of the upper 3 eV of the valence band ("weakly bonding") which is most strongly effected by the transition from the crystalline

into the amorphous phase, and 5) the existence of a high density of states ("bonding states") in the valence band starting approx. at 6 eV below the top of this band for both phases.

The photoemission data provide an explanation of the far UV reflectance spectra of Sb_2Se_3 which can be interpreted in terms of the joint density of states between the valence and conduction bands rather than in terms of single band densities of states [7]. Transitions from the upper 3 eV of the valence band are strongly polarization- and long-range-order-dependent, and they provide a large contribution to the optical transition strength in the photon energy region 1 to 35 eV. Particularly interesting are the sharp leading edges of the EDCs for both crystalline and amorphous Sb_2Se_3 which are in agreement with our previous findings from photoconductivity [8].

Since the photoemission measurements on clean specimens provide no information on the lower conduction band structure because of the high work function, additional photoemission measurements upon cesiated specimens will be performed allowing the sampling of an additional 4 eV of the conduction band.

4) Photoconductivity

Low temperature photoconductivity measurements have been performed on Sb_2Se_3. The detection of any IR photoresponse and/or band tailing was obviated by a strong, almost exponential, decrease of the photoresponse with decreasing temperature in case of amorphous Sb_2Se_3.

Thermopower measurements give the value of the Seebeck coefficient

reported previously for crystalline Sb_2Se_3 [9]. Strong polarization effects, probably similar to those reported for stibnite, Sb_2S_3, make the thermopower measurements unreproducible in the case of amorphous Sb_2Se_3.

5) ESCA Measurements

In collaboration with W. G. Proctor, Instrument Division, Varian Associates, extensive ESCA (electron spectroscopy for chemical analysis) measurements on crystalline and amorphous Sb_2Se_3 were made. The ESCA data essentially provide a measurement of the density of occupied states in the solid, in particular, of the valence band density of states. On the basis of the ESCA measurements we were able to eliminate any direct contribution of Sb 4d electrons to the optical properties in the range 0-25 eV as they lie at about 33 eV below the top of the valence band. Furthermore we were able to compare the ESCA results with $(h\nu)^2\epsilon_2$, the transition strength as obtained from the optical data. The data and their interpretation can be found in Appendix C. One important result obtained from the ESCA spectrum is the small change in valence band density of states upon the crystalline to amorphous transition.

B) Resistivity vs. Temperature Studies

ρ vs. T measurements for the three principle orientations of (zone refined) crystalline Sb_2Se_3 have been made. For any given crystal, the activation energy for all three principal orientations was equal within experimental error. The gap, Eg, of various samples though, ranged from 0.9 eV to 1.3 eV. The compositions of the crystals were obtained by

electron microprobe analysis. Tentative results show that the crystals with an E_g of 0.9 eV had a composition of 56% Se; those with an E_g of 1.3 eV had a composition of 61% Se. The bandgap of a 60% Se crystal was 1.06 eV. This shows the same qualitative trend in band gap vs. composition that was previously seen from optical and photoconductivity measurements on amorphous Sb_xSe_y films [8].

Preliminary ρ vs. T results on an amorphous film of Sb_2Se_3 showed the activation energy to be 0.65 eV.

C) Preparation and Characterization of Thin Amorphous Films

In the past six months we have isolated the major causes for the instability in rates of evaporation in our method for film preparation [10]. They were: 1) the manner in which the Electron Beam Gun (E.B. gun) power supply was used to focus and sweep the electron beam on the crucibles, and 2) the frequency shifts of the quartz crystal oscillator monitors used to control the rates of evaporation of the two sources. New improved, monitoring crystals are now being used and new techniques of sweeping the electron beam spot on the source material are being devised and implemented.

Because of the above improvements in our control of the relative rates of the sources we are now building a new evaporation system which will greatly increase the speed and completeness of our film studies. This system will employ two E.B. guns separated as far apart as the bell jar will allow. Three racks, at different heights, holding 30 substrates in a line will be suspended parallel to the axis of the two crucibles.

In this manner a series of films of different composition and thickness will be produced in a single run. Since each rack may be either at liquid N_2, room, or an elevated temperature, the system is applicable to any binary system within the scope of this study.

A series of films evaporated on substrates of different temperature is being studied to determine the effect of density (voids) on the dependence of the absorption coefficient upon energy. A determination of the substrate temperature at which Sb_2Se_3 forms a polycrystalline film will be made and comparison made with results of DTA measurements (see below). Measurements on the density of amorphous Sb_2Se_3 are also under way.

Modifications to the local fitting program described in the last semi-annual report were carried out to conduct inversions on measured reflectivity and transmission to obtain optical constants. The main improvement was a modification in the model of the optical system in the program to allow for the finite halfwidth of the light incident on the specimen. To overcome this problem, it was necessary to invert the data over a wavelength distribution function with a halfwidth comparable to that of a Cary 14 spectrophotometer. A Calcomp routine to plot optical data was devised in order to facilitate handling large quantities of data.

') Differential Thermal Analysis

Differential thermal analysis of an amorphous film of Sb_2Se_3 produced by a single source evaporation was conducted between 24° C. and 250° C. The rate of heating was 0.5° C./min throughout the experiment. The only

structure noted was an exothermic peak which began at 160° C. and had a maximum at 178° C. This was assumed to be the amorphous to crystalline transition. The specific heat of the amorphous sample was 1.9 joules/gm from 25° C. to 150° C. After crystallization, the specific heat was 4.2 J/gm in the range 180° C. to 220° C. An indication of the glass transition temperature was sought, but not found in this temperature range.

III. RESEARCH ON Sb_2O_3 AND Sb_2Te_3

A) Sb_2Te_3

A number of Sb-Te films of varying composition have been produced. We must wait until the new evaporation system mentioned above is complete in order that discrepancies in the optical data for this system can be clarified. Preliminary measurements indicate substantial differences between crystalline and amorphous materials.

Strong degeneracy of crystalline Sb_2Te_3 obviates any observable photoresponse even at liquid nitrogen temperature. In the case of amorphous Sb-Te films cooling of samples results in photoresponse indicating the bandgap at approx. 0.7 eV. However, additional measurements on other samples of well defined composition are necessary.

Our preliminary photoemission spectra of Sb_2Te_3 in the 7 to 15 eV region shows very strong effects due to free carriers which obscure most of the band structure. These same effects obscure the structure from interband transitions in the reflectivity.

B) Sb_2O_3

Two films of Sb_2O_3 (thin and thick) were produced by evaporation and optical absorption measurements are being made on them.

Orthorhombic needles, cubic crystals, and an amorphous film were grown by vapor transport and their optical properties measured near their absorption edge (2-4 eV). A preprint of this work is attached as Appendix D.

Attempts to grow larger orthorhombic needles are presently in progress. Photoconductivity measurements on both amorphous and crystalline Sb_2O_3 are being initiated.

In addition zone refining to produce single crystals of Sb_2S_3 and As_2Te_3 is under way.

IV. STRUCTURAL INVESTIGATIONS

A) X-ray and Electron Diffraction

The electron diffraction work on amorphous Sb_xSe_y [11] amorphous films has been extended to temperatures as low as -120^{o} C. Amazingly, the samples crystallized in an intensive electron beam even at low temperatures. Local heating by the electron beam due to low conductivity of the specimen may have taken place. In addition to the patterns typical at room temperature, a superlattice was observed.

The $Sb_2Se_xTe_{3(1-x)}$ single crystal work by X-ray diffraction has been continued. The atom parameters were determined from the (00ℓ) reflections by use of a least squares refinement program. The parameters so obtained for pure Sb_2Te_3 were $u_{Sb} = 0.400$ and $u_{Te} = 0.787$ as compared with 0.400 or 0.789, respectively, listed in the literature. The R-factor, a measure for the reliability of the data, was 0.214. It was furthermore attempted to determine into which of the two Te positions, (0,0,0) or (0,0,u) the Se atom goes. While the range of composition, ($SbTe_3$ - $Sb_2Se_2Te_1$) for which mixed single crystals can be obtained seemed to indicate that only substitution of the Te in the (0,0,u) positions occurs (case I), researchers have suspected a different type of Se distribution on account of the physical behavior. In particular, it has been assumed that only after the (0,0,0) position is completely filled up by Se, and excess Se goes into the (0,0,u) position (case II). Our data indicate that probably the first of these cases occurs. The Se parameter was determined as $u_{Se} = 0.778$. We obtained an R-factor of 0.343 for the case I as compared with an R-factor of 0.713

for case II. Calculations for a completely statistical arrangement of Se in both of the Te positions resulted in an R-factor of 0.382. This statistical arrangement is not very different from case I for Se rich samples such as $Sb_2Se_2Te_1$. Presently attempts are being made to obtain an even better agreement between experimental and calculated data by proper determination of the individual temperature factors.

B) Mossbauer Spectroscopy

The feasibility of obtaining useful information on the chemical bond of antimony by means of the Mossbauer Effect has been demonstrated by Ruby and his co-workers [12,13,14]. A Mossbauer investigation at Sb^{121} nuclei will be conducted to examine the antimony bond in the amorphous systems Sb_2Te_3 and Sb_2S_3. The electronic structure and local crystal symmetry will be contrasted with that of the crystalline compounds [15]. The Mossbauer isomer shift reflects the character and number of valence electrons; the quadrupolar splitting both the degree of local order and the character of the valence electrons. Thus, the isomer shift and quadrupolar coupling parameters can be interpreted in terms of electronic structure. The isomer shift will be correlated with the electron density [16] (calculated from Hartree-Fock wave functions) at the Sb^{121} nucleus to obtain the electronic structure of antimony in amorphous Sb_2Te_3 and Sb_2S_3. The relationship between the isomer shift and quadrupole splitting will be used as a further check on electronic structure.

An experiment has been designed to measure the Mossbauer effect at Sb^{121} nuclei in both the superconducting and normal forms of amorphous

antimony. A special dewar has been constructed so that amorphous antimony sample can be deposited on quartz substrate at liquid nitrogen temperature. The dewar can then be transferred to a Mossbauer spectrometer, while the sample is retained at liquid nitrogen temperature. Possible correlation between local symmetry at Se atoms predicted from the results of mass spectrographic analysis of the constituents of each amorphous form and the quadrupolar coupling will be studied.

REFERENCES

1. R. Afshar, F. M. Mueller and J. C. Shaffer, J. Comp. Phys. (in press).
2. M. V. Romerio, J. Math. Phys. 12, 552 (1971).
3. C. Wood, Z. Hurych and J. C. Shaffer, J. Non. Cryst. Solids (in press).
4. E. Mooser and W. B. Pearson, J. Phys. Chem. Solids 7, 65 (1958).
5. N. W. Tideswell, F. H. Kruse, and J. D. McCullough, Acta, Cryst. 10, 99 (1957).
6. Boyd Veal (private communication).
7. R. E. Drews, R. L. Emerald, M. L. Slade and R. Zallen, Sol. St. Comm. 16, 293 (1972).
8. Z. Hurych, R. Mueller, C. C. Wang, C. Wood, J. Non. Cryst. Solids, in press.
9. J. Black, E. M. Conwell, L. Seigle, and C. W. Spencer, J. Phys. Chem. Solids, 2, 240 (1957).
10. R. Mueller and C. Wood, J. Non. Cryst. Solids (in press).
11. H. B. Krause (to be published).
12. S. L. Ruby and G. K. Shenoy, Phys. Rev. 186, 326 (1969).
13. S. L. Ruby, G. M. Kalvius, G. B. Beared, and R. E. Snyder, Phys. Rev. 159, 239 (1967).
14. S. L. Ruby, L. Gilbert and C. Wood, Phys. Ltrs., 37A, 453 (1971).
15. S. P. Taneja, A. E. Dwight, L. Gilbert, W. C. Harper, C. W. Kimball, and C. Wood, Phys. and Chem. of Glasses (in press).
16. D. A. Shirley, Rev. Mod. Phys. 36, 339 (1964).

FISCAL STATUS

	Amount Allocated	Amount Spent	Balance
Personnel	$38,995.00	$37,506.44	$1,488.51
Supplies, Expenses and Services	$11,984.00	$12,519.05	- $ 535.05
Travel	$ 1,500.00	$ 955.13	$ 544.87
		TOTAL BALANCE	$1,498.33

APPENDIX A

Electronic Structure of Single Crystal and Amorphous Sb_2Se_3*

J. C. Shaffer, B. Van Pelt and C. Wood
Physics Department
Northern Illinois University
DeKalb, Illinois 60115

and

J. Freeouf, K. Murase, and J. W. Osmun
Physics Department
University of Chicago
Chicago, Illinois 60637

ABSTRACT

The near normal incidence reflectivity of Sb_2Se_3 has been measured upon both crystalline and amorphous samples. The data was obtained for two polarizations ($\vec{E}||a$, $\vec{E}||c$) in the cleavage plane of the crystal. The data was Kramers-Kronig analyzed and the implications of the results regarding the electronic structure of the compound were interpreted in terms of a valence bonding model. In particular the valence band electrons divide into those in weakly bonding resonance states and those in covalent bonding states. Upon the amorphous to crystalline transition it is the optical transitions originating in the former which appear to be principally influenced.

The optical properties of single crystal and amorphous Sb_2Se_3 have been measured in the energy range 0 to 24 eV in order to characterize

---

*This work was supported by the Advanced Research Projects Agency of the Department of Defense and was monitored by the Army Research Office, Durham, under Contract No. DA-ARO-D-31-124-71-G132. We wish, also, to acknowledge support by the U.S. Air Force Office of Scientific Research under contract numbers F44620-71-C-0025 and F44620-70-C-0029.

the influence of long range order on the electronic structure in this compound.

Crystalline Sb_2Se_3 is orthorhombic ($a = 11.62\mathring{A}$ $b = 11.77\mathring{A}$ $c = 3.96\mathring{A}$) [1] of space group D_{2h}^{16}, type D_8^5, with 20 atoms, i.e., 4 molecules/unit cell. The atoms are arranged in a layer structure with layers $\perp b$ and weak Sb-Se bonding [1] between layers and, therefore, the crystals exhibit natural cleavage $\perp b$. Excellent mirror-like surfaces for optical studies with polarizations $\vec{E} \| a$ and $\vec{E} \| c$ can be prepared by cleaving. However, great difficulty is experienced in preparing good surfaces perpendicular to the cleavage plane because the crystals are soft and easily deformed. Slight surface oxidation occurs if the crystals are exposed to air for long periods (days). Hence, all optical samples were either freshly cleaved or kept under an argon atmosphere prior to measurement.

Single crystals of Sb_2Se_3 were grown in a zone refiner [2] from 6-9's purity elements after extensive zone refining of the compound. Amorphous films of Sb_2Se_3 were prepared by controlled coevaporation of the elements [3] onto room-temperature fused quartz substrates.

Various spectrophotometers having overlapping energy ranges were used to cover the energy range 0 to 24 eV and comprised: a Cary 14R (0.4 eV to 6 eV); a McPherson 225 with Hinteregger Light Source [4] (4 to 12 eV); a McPherson 235 with Synchrotron Radiation Source (4 to 24 eV). Optical reflectivity was measured using the following apparatus: a Cary Model 1413 Reflectance Attachment (0.4 to 6 eV); a McPherson Reflectance

Attachment (4 to 12 eV); reflectance apparatus described in [5] (4 to 24 eV). Sheet polarizers were used in the range 0.4 to 6 eV (Polaroid HR and Polarcoat ultraviolet polarizers). The naturally occurring polarization of about 80% in the Synchrotron radiation and reflectance attachment obviated the need for polarizers in the range 4 to 24 eV.

The room-temperature reflectivity at near normal incidence of single crystal Sb_2Se_3 in the energy range 0 to 5 eV is shown in Fig. 1 for both $\vec{E}||a$ and $\vec{E}||c$. This data represents the maximum values obtained from measurements taken on five different single crystal samples of Sb_2Se_3. The reflectance values of the various samples were found to lie within a range ±2%.

The structure displayed by the single crystals in the range of the broad reflectivity maxima, 1 to 6 eV, is in good general agreement [6] with the data of Shutov et. al. [7] (see Table 1) and is a result of critical points in the joint density of states. The spectrum of Sb_2Se_3 near the absorption edge indicates that the extremes of the valence and conduction bands occur at different points in the zone and that absorption begins with an indirect transition at 1.16 eV [8]; this is appreciably higher than the value of 0.89 eV reported by Sobolov et. al. [9]. From symmetry considerations on isostructural Sb_2S_3, Audzijonis et. al. [10] have suggested that the maximum of the valence band at the center of the Brillouin Zone Γ is split into subbands Γ_2, Γ_6 and Γ_4. Correspondingly, Sobolov et. al. have associated transitions between $\Gamma_2(\vec{E}||a)$, $\Gamma_6(\vec{E}||b)$, $\Gamma_4(\vec{E}||c)$, and the state Γ_1 at the conduction band minimum with the lowest direct transition in Sb_2Se_3. No assignments have been made for the higher energy structure in the broad reflectivity maximum.

In marked contrast, the broad reflectivity maximum of the amorphous form of Sb_2Se_3 is featureless showing that the selection rules for these transitions are broken and/or the critical point structure in the densities of states is greatly smoothed in the absence of long range order. In addition, as has been found in other V-VI [11] compound semiconductors as well as Te [12], the reflectance of the amorphous material is significantly lower than that of the crystal in the visible to near ultraviolet spectral range.

The near normal incidence reflectance measured in the range 4 to 24 eV using synchrotron radiation is shown in Figure 2. At energies greater than 8 eV, a marked similarity exists between the reflectance of the crystalline and amorphous samples. The minima at 8 eV closely correspond to those of As_2S_3 and As_2Se_3 [11] and similarly, by Kramers-Kronig analysis, appear to be associated with the threshold of a new absorption process from a deeper lying valence band. In the region of this second broad maxima, two marked peaks are observed at 10 and 12.4 eV independent of the orientation of the $\vec{E}$ vector or the absence of long range order.

The normal incidence reflectivity data up to 24 eV described above have been Kramers-Kronig analyzed by the method described by Afshar et. al. [13] [14]. The method essentially consists of two steps. First the Kramers-Kronig relation between the phase and the modulus of the complex reflection coefficient

$$\phi(\omega) = \frac{P}{\pi} \int_{-\infty}^{+\infty} \frac{\ln r(\omega')\, d\omega'}{\omega' - \omega} \qquad (1)$$

is separated into two portions, i.e., $\phi(\omega) = \chi(\omega) + \theta(\omega)$, where

$$\chi(\omega) = \frac{P}{\pi} \int_{-\infty}^{+\infty} \frac{\ell n \rho(\omega')\, d\omega'}{\omega' - \omega} \tag{2}$$

and

$$\theta(\omega) = \frac{P}{\pi} \int_{-\infty}^{+\infty} \frac{\Delta(\omega')\, d\omega'}{\omega' - \omega} \,. \tag{3}$$

In these relations $\rho(\omega')$ is the modulus of the complex reflectivity for a system of charged classical harmonic oscillators chosen to have a reflectivity $\rho^2(\omega')$ which closely fits the measured reflectivity data at the high and low frequency extremes of the measured range. $\rho^2(\omega')$ thus extrapolates the data into the unmeasured spectral regions. The $\chi(\omega)$ can easily be computed from the appropriate dielectric function (which gives rise to $\rho^2(\omega')$) of the form

$$\varepsilon(\omega) = 1 + \sum_{i=1}^{N} \frac{f_i}{(\omega_i^2 - \omega^2) + i\Gamma_i\omega} \tag{4}$$

where the constants (f_i, Γ_i) parametrize the strength and linewidth of the classical oscillator with resonant frequency ω_i. In the analysis of the data presented here two oscillators are sufficient to fit the data at the extremes of the data range. $\theta(\omega)$ is computed by expanding $\Delta(\omega')$, the residual portion of $\ell n\, r(\omega')$, in Hermite functions, and using the Hermite representation of the Hilbert transform operator developed by Afshar et. al. [13] to compute the integral in (3). All optical functions are obtainable from $\rho(\omega)e^{i\phi(\omega)}$, the complex reflection coefficient.

In Fig. 3 the imaginary part of the dielectric function, $\varepsilon_2(\omega)$, is shown for the two polarizations $\vec{E}||a$, and $\vec{E}||c$ and for the amorphous film as computed from the reflectivity data above. In Fig. 4 the same display is made for $\varepsilon_1(\omega)$ and Fig. 5 shows a plot of the energy loss function $-\mathrm{Im}\,\frac{1}{\tilde{\varepsilon}}$ in each case.

An additional interesting feature is the comparison of the sum rules on $\sigma_1(\omega) = \omega\varepsilon_2(\omega)$ for the three cases. Thus we have computed

$$\frac{2}{\pi} \int_0^{\omega} \omega' \, \varepsilon_2 \, (\omega') \, d\omega' = \frac{4\pi e^2}{m} \frac{4}{\Omega} \, n(\omega), \tag{5}$$

in each case, where $n(\omega)$ is the number of electrons per molecule participating in transitions up to frequency ω, and Ω is the unit cell volume. Fig. 6 shows $n(\omega)$ for both polarizations for the crystal as well as for the amorphous film. In each instance there is a discernible inflection in $n(\omega)$ between 7.0 and 8.0 eV beyond which $n(\omega)$ rises sharply with the onset of the A_{11} and A_{13} peaks. The inflection is slightly obscured for $\vec{E}||c$ by the A_9 peak as one might expect from Figs. 2 and 3. These results are similar to those reported on As_2Se_3 and As_2S_3 in [15]. In all cases, however, $n(\omega)$ attains a value of about 25 → 26 electrons/molecule for ω = 24 eV. Since each molecule of Sb_2Se_3 nominally contributes 28 valence electrons it is assumed that the sum rule will saturate at an energy slightly greater than 24 eV at 28 electrons/molecule.

It is reasonable to assume that the transitions which dominate up to 8 eV involve electrons associated with the weak resonating p-bonds which were hypothesized by Mooser and Pearson [16] to occur in Sb_2Se_3 on the basis of the structural determinations of Tideswell et. al. [17]. At energies greater than about 8 eV the onset of transitions from the energetically lower states associated with covalent bonds occurs. Study of the $n(\omega)$ curves in Fig. 6 indicates that the lower frequency portion would saturate at about 16 electrons/molecule and the higher frequency portion, of course, at an additional 12 electrons/molecule. This compares favorably with the number of electrons/molecule associated with weaker and stronger bonds in Table 6 of [1].

The suppression of the reflectivity of the amorphous sample in the visible and near ultra-violet arise from sensitivity of the transitions from the resonating p-bonds to the lack of long range order. This could result from a reduction of the average matrix element for these transitions or from reduction of the density of states in the conduction or valence bands in the appropriate energy range. ESCA measurements [17] on amorphous and crystalline Sb_2Se_3 indicate quite small differences in the magnitude of the valence band density of states in the energy range of interest. Thus this effect seems to be associated either with reduced matrix elements in the amorphous material or with some influence of the disorder on the conduction band density of states, perhaps through a reduction of Sb 5d-band overlap contributions.

The ESCA data also locates the 4d bands of Sb at 33 eV below the top of the valence band thus obviating any direct influence of these levels on the optical properties in the spectral range studied. The results reported here on the sum rule confirm this.

As a check upon the accuracy of the Kramers-Kronig analysis and our low-frequency extrapolations of reflectivity we have directly computed $\varepsilon_1^f(0,\omega)$, the "frequency-dependent" static dielectric constant, from the Kramers-Kronig formula

$$\varepsilon_1^f(0,\omega) = 1 + \frac{2}{\pi}\int_0^{\omega} \frac{\varepsilon_2(\omega')\, d\omega'}{\omega'} \quad ,$$

where $\varepsilon_2(\omega)$ is the imaginary part of the dielectric function obtained from our Kramers-Kronig analysis of reflectivity. Since $\varepsilon_1(0)$ is fixed by the value of reflectivity in the low frequency limit we can compare $\varepsilon_1^f(0,\omega)$ with $\varepsilon_1(0)$. In every case we find that $\varepsilon_1^f(0,\omega)$ approaches the

$\varepsilon_1(0)$ value assumed by extrapolating $R(\omega)$ to low frequency and is equal to $\varepsilon_1(0)$ within 5% at the upper end of our data range. $\varepsilon_1^f(0,\omega)$ is found to be smaller for the amorphous sample reflecting the smaller overall magnitude of the low frequency reflectivity in this case.

To summarize, the following points are to be emphasized. In comparison with the work of Shutov et. al. [10] this study shows some differences in the exact location of certain of the critical point structure in the reflectance of crystalline Sb_2Se_3 (see Table I). In general, however, the agreement is quite close in the overlapping region studied. In regard to comparison of the amorphous and crystalline samples it is seen that the absorption, as characterized by $\varepsilon_2(\omega)$, e.g., shows nearly complete smearing of the critical point structure in the amorphous material in the visible and near ultraviolet. Furthermore there is an overall suppression of the absorption in comparison with that of the crystalline samples in this range. Beyond about 8.0 eV the spectra of the crystalline material (for either polarization) and the amorphous film are virtually identical. The close similarity of the energy loss function, $-\mathrm{Im}\,\frac{1}{\varepsilon}$ for the three cases (there is a near coincidence of the valence-band plasma peaks at about 17 eV) suggests that the occupied bands have similar overall properties in the amorphous and crystalline material, e.g., number of states/volume and average effective mass. We conclude, therefore, that the influence of the lack of long range order upon the electronic structure of Sb_2Se_3 is confined, for all practical purposes, to the conduction bands and higher valence bands of the material, and that loss of long range order alters the weakly bonding resonance electron states producing a substantial change in the optical properties.

ACKNOWLEDGEMENTS

We wish to thank H. Fritzsche for his valuable comments and suggestions and the staff of the Wisconsin Physical Science Laboratory for their experimental assistance.

REFERENCES

1. N. W. Tideswell, F. H. Kruse and J. C. McCullough, Acta Cryst. 10, 99 (1957).

2. C. Wood, B. Van Pelt and E. Hyland (to be published).

3. R. Mueller and C. Wood, J. Non-Cryst. Solids (in press).

4. Instrument loaned by Dr. P. Yuster, Solid State Div., Argonne National Laboratory.

5. U. Gerhardt and G. W. Rubloff, Appl. Opt. 8, 305 (1969), G. W. Rubloff, H. Fritsche, U. Gerhardt, and J. Freeouf, Rev. Sci. Instr. 42, 1507 (1971).

6. C. Wood, Z. Hurych and J. C. Shaffer, J. Non-Crystalline Solids (in press).

7. S. D. Shutov, V. V. Sobolov, Y. V. Popov and S. N. Shestatskii, Phys. Stat. Sol. 31 K23 (1969).

8. B. Van Pelt and C. Wood (to be published).

9. V. V. Sobolov, S. D. Shutov and S. N. Shestatskii, Moldavian Academy of Sciences, U.S.S.R., 183 (1969).

10. A. Audzijonis, J. Batarunas, A. Karpus and S. Kudzmanskas, Lietuvos Fizikos Rinkiny 5 481 (1965).

11. R. Zallen, R. E. Drews, R. L. Emerald and M. L. Slade, Phys. Rev. Lett. 26 1564 (1971).

12. J. Stuke, J. Non. Cryst. Solids 4 1 (1970).

13. R. Afshar, F. M. Mueller and J. C. Shaffer, J. Comp. Phys. (in press).

14. R. Afshar, F. M. Mueller and J. C. Shaffer (to be published).

15. R. E. Drews, R. L. Emerald, M. L. Slade and R. Zallen, Sol. St. Comm. 16, 293 (1972).

16. E. Mooser and W. B. Pearson, J. Phys. Chem. Solids, 7 65 (1958).

17. C. Wood, J. C. Shaffer and W. V. Proctor (to be published).

Table 1 Reflectivity peaks energies (eV) of Sb_2Se_3*

Polarization	A_1	A_2	A_3	A_4	A_5	A_6	A_7	A_8	A_9	A_{11}	A_{12}	A_{13}
$\vec{E}\|\|a$	1.36 (1.36)	2.00 (1.97)	-- --	-- --	3.30 (3.15)	4.15 (3.95)	-- (4.56)	-- (5.6)	(7.4) 7.4	10.0 (9.5)	-- (10.8)	12.4 --
$\vec{E}\|\|c$	-- --	-- (1.90)	2.30 (2.30)	3.00 (2.95)	-- (3.20)	4.0 (4.0)	4.52 (4.52)					

* The bracketed data is that of Shutov et. al. [7].

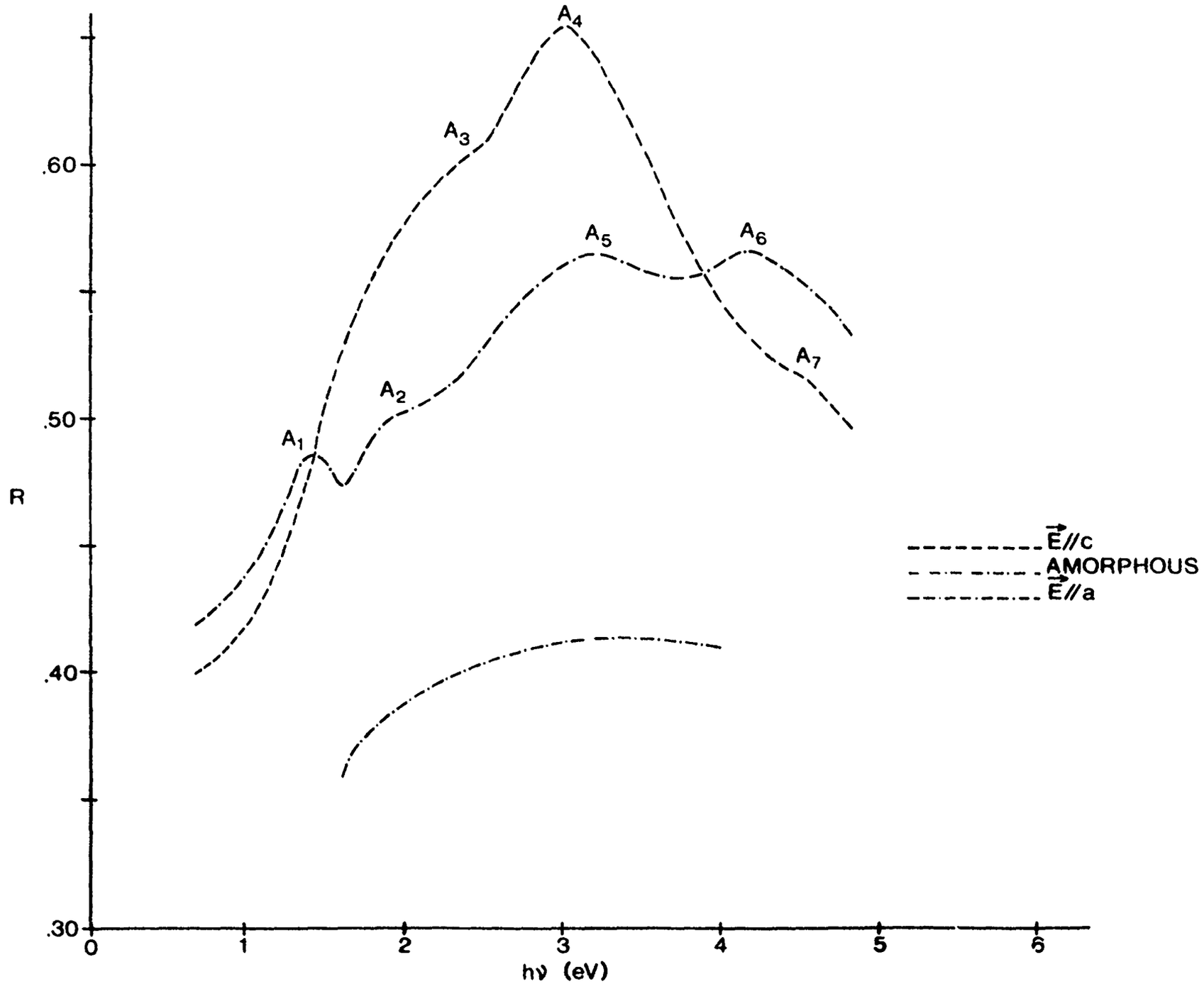
A4
A3
A5
A6
A7
A2
A1
.60
.50
.40
.30
R
0
1
2
3
4
5
6
hν (eV)
E//c
AMORPHOUS
E//a

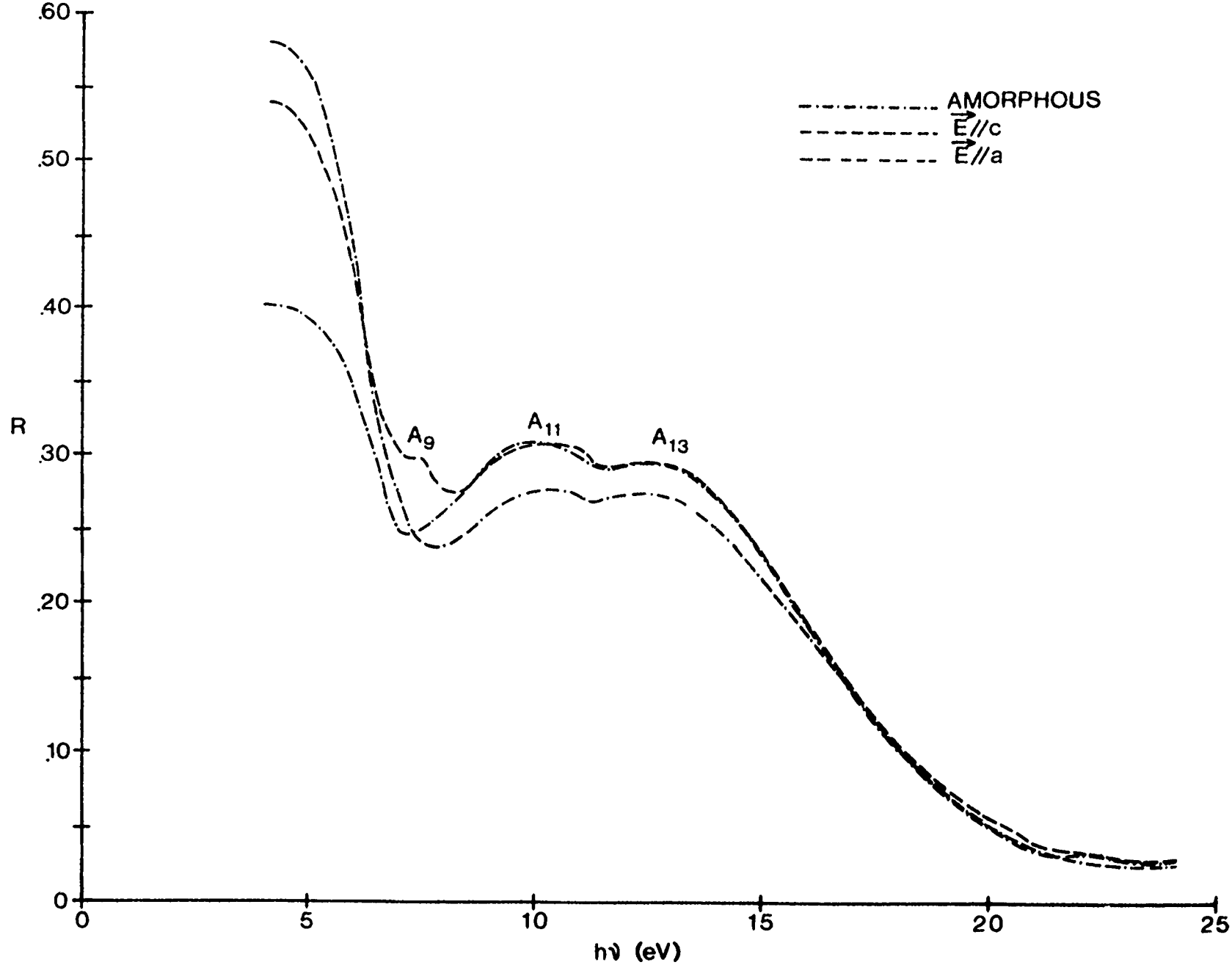
.60
.50
.40
.30
.20
.10
0
R
0
5
10
15
20
25
hν (eV)
A9
A11
A13
AMORPHOUS
E//c
E//a

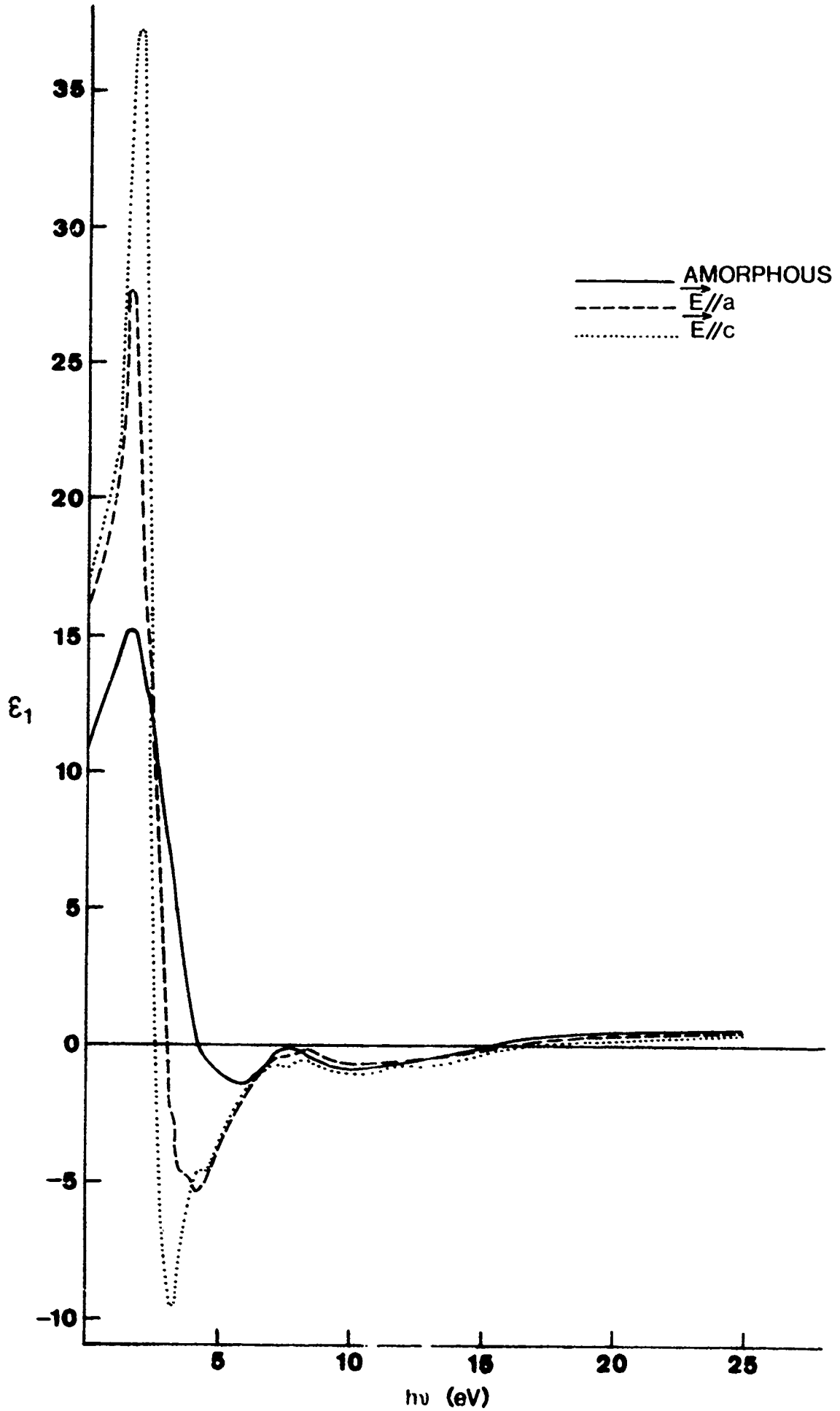
35
30
25
20
15
10
5
0
-5
-10
ε_1
5
10
15
20
25
hν (eV)
AMORPHOUS
E//a
E//c

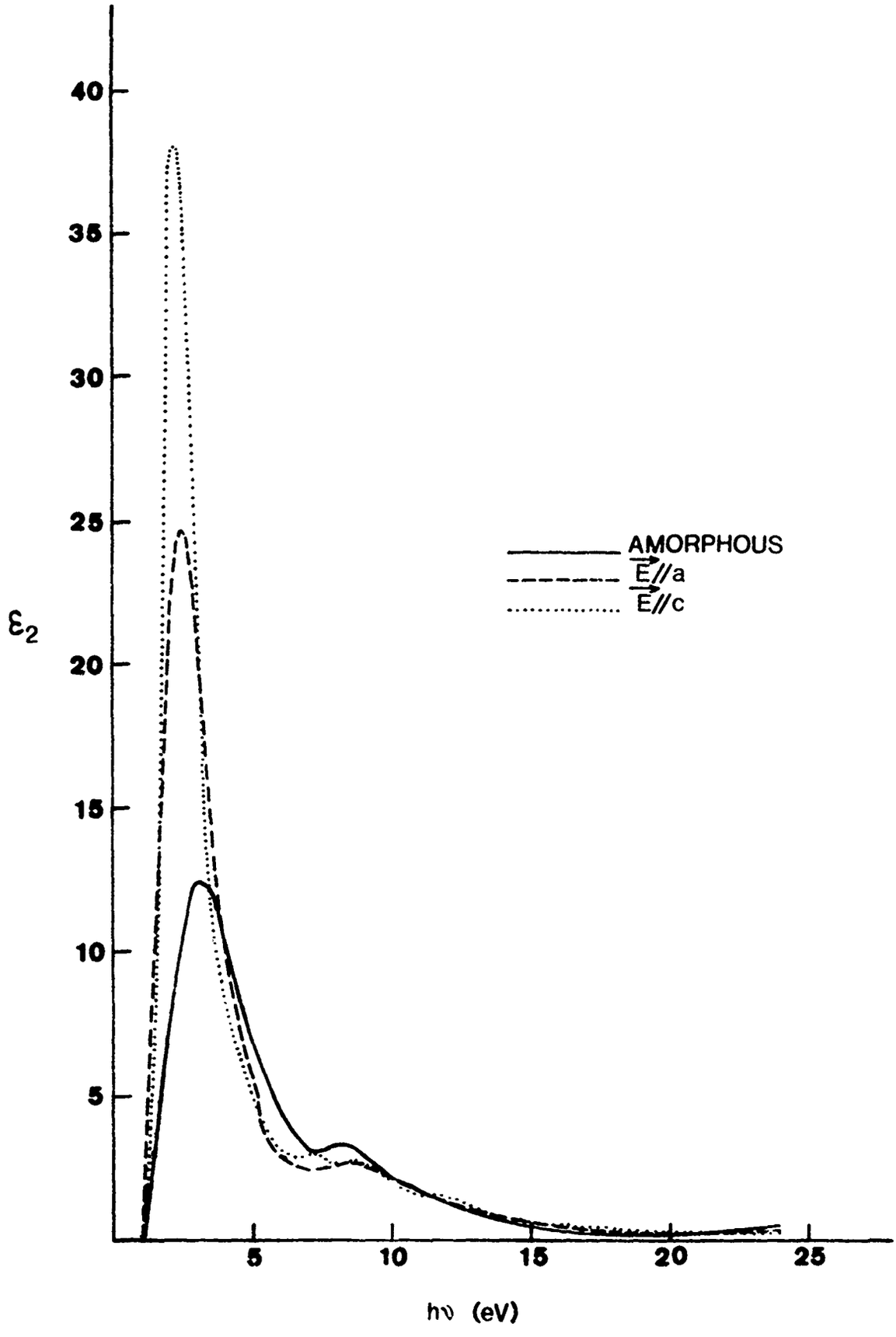
40
35
30
25
20
15
10
5
ε_2
AMORPHOUS
$\vec{E}$//a
$\vec{E}$//c
5
10
15
20
25
hν (eV)

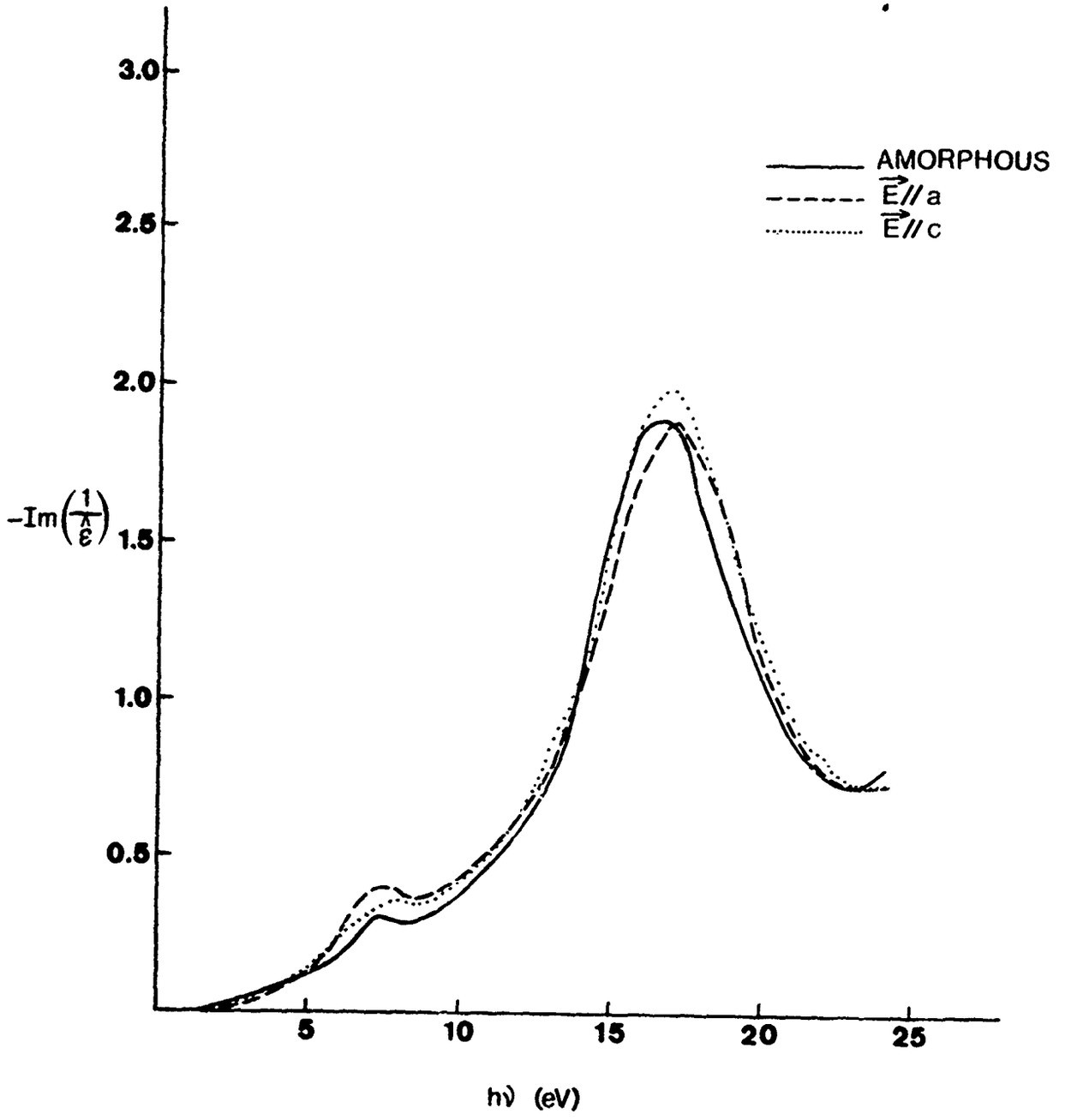
3.0
2.5
2.0
1.5
1.0
0.5
$-\mathrm{Im}\left(\frac{1}{\varepsilon}\right)$
AMORPHOUS
$\vec{E}$// a
$\vec{E}$// c
5
10
15
20
25
hν (eV)

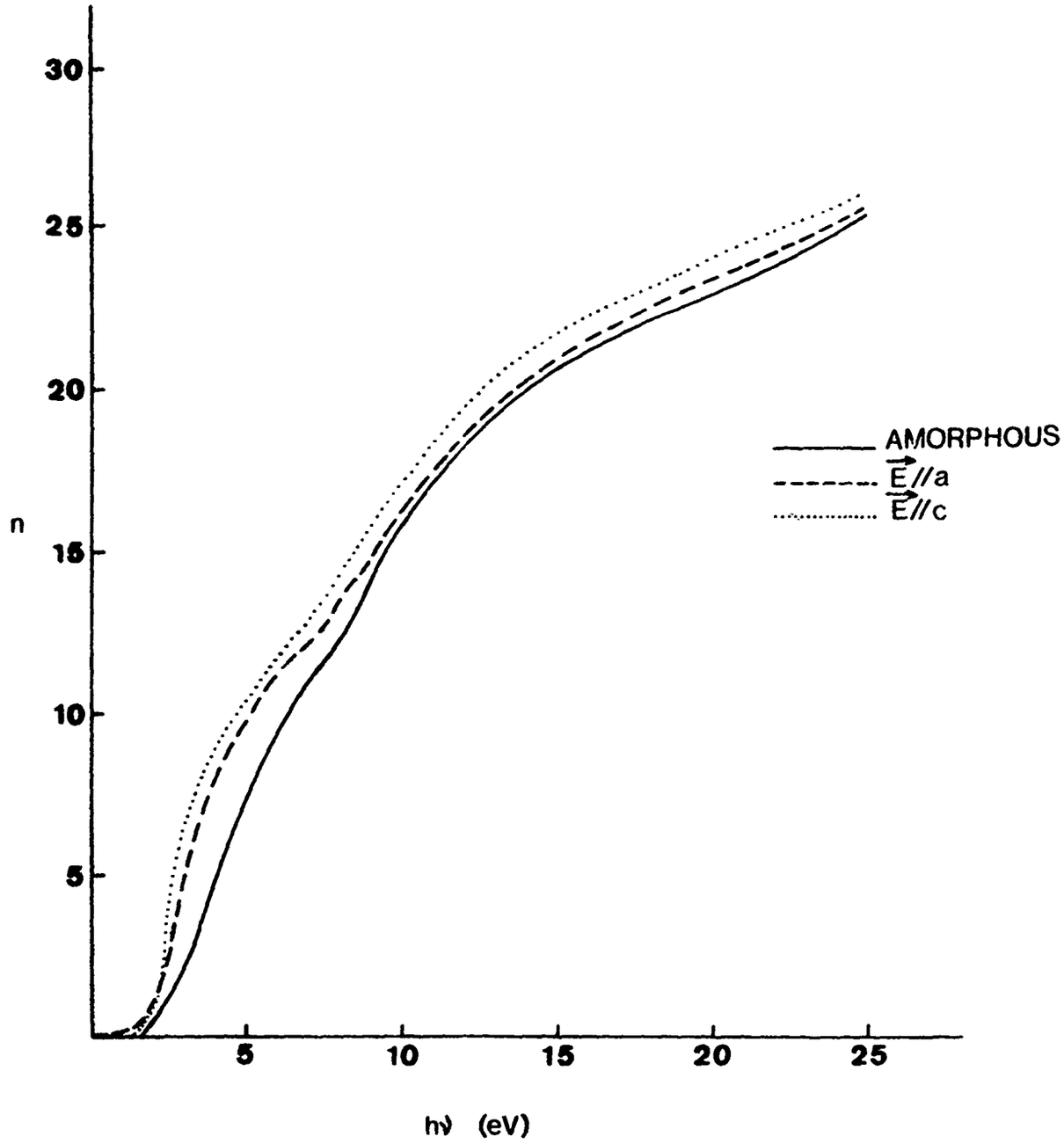
30
25
20
15
10
5
n
5
10
15
20
25
hν (eV)
AMORPHOUS
E//a
E//c

APPENDIX B

Photoemission Studies of Crystalline and Amorphous Sb_2Se_3

Z. Hurych, D. Buczek and C. Wood†
Physics Department
Northern Illinois University
DeKalb, Illinois 60115

and

G. Lapeyere and A. Beyer
Physics Department
Montana State University
Bozeman, Montana 59715

† This work was supported by the Advanced Research Projects Agency of the Department of Defense and was monitored by the Army Research Office, Durham, under Contract No. DA-ARO-D-31-124-71-G132. We wish, also, to acknowledge the support of the Synchrotron Radiation Laboratory, University of Wisconsin, under Air Force contract No. F44620-70-C-0029.

ABSTRACT

The synchrotron storage ring was used as a source of polarized UV radiation for performing the high resolution (0.2 eV in the whole 7 eV to 40 eV region) photoemission spectroscopy of crystalline and amorphous Sb_2Se_3. Resulting EDCs for crystalline Sb_2Se_3 are strongly polarization dependent and show peaks corresponding to the initial energy of states at 0.8, 1.7, 2.6 and 3.3 eV below the top of the valence band as well as a larger density of final states in the region 6.5 eV to 9.5 eV above the top of the valence band. Amorphous Sb_2Se_3 exhibits one broad peak approx. 1.5 eV below the top of the valence band and structure in the final states at about 7.7 eV above the top of the valence band. An additional increase of the valence band density of states occurs at about 6 eV below the top of the valence band for both crystalline and amorphous Sb_2Se_3. The typical reflectivity structure of V-VI compounds between 7 eV and 15 eV attributed to the splitting of the valence band into bonding and nonbonding states can be explained from the EDCs in terms of the JDOS between the valence and conduction bands rather than in terms of a single band structure for both amorphous and crystalline Sb_2Se_3, in the latter being further enhanced by matrix elements for direct transitions.

INTRODUCTION

The typical features of the reflectivity spectrum of Sb_2Se_3, and of several other V-VI compound semiconductors, in both crystalline and amorphous form are the two reflectivity bands, the first occurring in the near IR and visible region, and the second in the vacuum UV region of the spectrum with onset at ∿7 eV (1), (2), (3). The overall reflectivity spectrum with the two reflectivity bands has been recently interpreted (4) (5) as originating from the splitting of the valence band into strongly bonding and weakly bonding states. Since this splitting of the valence band seems to be a general feature of most V-VI compounds, as suggested by the reflectance spectra, more detailed knowledge of the valence band structure should certainly be useful in explaining many physical properties of these materials. However, the reflectivity and resulting optical constant ϵ_2 provide only the joint density of states (JDOS) without localizing absolutely either the initial or the final energy of states involved. In addition, it is generally difficult to determine what structure in the optical data is due to the density of states in a band and what is due to enhancement by matrix elements at critical points of Brilloin zone, the later contribution being generally unimportant in amorphous materials as a result in our case since the far UV reflectivity structure (7 to 15 eV) is very similar for both amorphous and crystalline Sb_2Se_3 (1) (5), As_2Se_3 and As_2S_3 (3). In order to obtain the answer to these two questions, the photoemission spectroscopy technique was employed which gives both the absolute energy level of states (EDJDOS), i.e., the energy distribution of JDOS is measured)

as well as the provision to distinguish between direct and nondirect transitions. Since Sb_2Se_3 is a strongly anisotropic material, a need for polarized light used to excite electrons seems obvious. Naturally polarized light from the storage ring of a synchrotron was used as a source of exciting radiation; this arrangement also extended the photon energy range up to 40 eV. Our results on crystalline Sb_2Se_3 confirm the importance of the use of polarized light in case of optically anisotropic materials.

PHOTOEMISSION AND OPTICAL DATA

The optical data and their Kramers-Kronig transform are associated with the joint lensity of states (JDOS) weighted by the transition probability, i.e., by the square of dipole excitation matrix elements $M_{if}(\underline{k},\hbar\omega)$. The JDOS represents the total number of direct transitions which can take place for given photon energy $\hbar\omega$, and is given by eq. (1).

$$JDOS(\hbar\omega) = (2\pi)^{-3} \sum_{i,f} \int d\underline{k}\ \delta(E_f(\underline{k}) - E_i(\underline{k}) - \hbar\omega). \qquad (1)$$

The contribution of these interband transitions to the optical functions is described by the optical transition strength $\omega^2\varepsilon_2$ given as

$$\omega^2\varepsilon_2 = B \sum_{i,f} \int d\underline{k} |M_{if}(\underline{k},\hbar\omega)|^2\ \delta(E_f(\underline{k}) - E_i(\underline{k}) - \hbar\omega) \qquad (2)$$

where $E_i(\underline{k})$ and $E_f(\underline{k})$ are the electrons energies of the initial filled and final empty states, and B is a constant. In semiconductors the integration is restricted to $E_i(\underline{k})$ below the valence band maximum and to $E_f(\underline{k})$ above the conduction band minimum. In the constant matrix elements approximation (where one assumes no dependence of M_{if} on $\underline{k}$) and in the case of nondirect transitions (where $\underline{k}$ is not a significant quantum number, which is the case in many amorphous materials), the integration in eq. (2) can be easily performed and the optical transition strength can be then expressed in terms of the valence and conduction band densities of states N_v and N_c as

$$\omega^2\varepsilon_2 = B' \int M^2\ N_v(E - \hbar\omega)N_c(E)\ dE. \qquad (3)$$

Here B' is a constant, and M^2 is a slowly varying function of $\hbar\omega$. The M^2 dependence can be then included in N_c and N_v to define the optical densities of states $N_c' = MN_c$ and $N_v' = MN_v$. The electrons energy E in eq. (3) is then measured from the top of the valence band. While the $\omega^2\varepsilon_2$ is related to

the total number of photoelectrons excited by photon of energy $\hbar\omega$, one is often interested in the quantity EDJDOS, i.e., the energy distribution of the JDOS. Such quantity is obtained from the photoemission experiments which provide the energy distribution curves (EDC) at any given photon energy $\hbar\omega$. The EDCs provide the energy distribution of the JDOS weighted by matrix elements and modified by the escape function $T(E,\underline{k})$. In the case of constant matrix elements one can write

$$EDC(E,\hbar\omega) = B' M^2 N_v(E - h\omega) N_c(E) T(E,\underline{k}) \qquad (4)$$

for $\phi \leq E \leq h\omega$, where ϕ is the work-function. The effective escape function $T(E,\underline{k})$ includes both the transport and escape of the photoexcited electrons. As such it includes the mean free path of hot electrons l, the optical-absorption coefficient α, and the threshold function $T'(E)$. The $\underline{k}$ dependence of T which introduces an anisotropy of T is primarily a result of the relation $l = \tau|\nabla_k E|h^{-1}$ where τ is the scattering time. The threshold function $T'(E)$ can be in the simplest case thought of as a step function (6) or as a monotonically increasing function of $(E - \phi)$ for $E > \phi$ (7), and therefore can have generally different values for different crystal faces. Since in our experiment the same cleaved surface (0,1,0) was used for both polarizations $E_o \| a$ and $E_o \| c$, the threshold function $T'(E)$ is in our case polarization independent. Inspection of all quantities comprising the expression for the EDJDOS shows that the only two terms which can be dependent on the orientation of the electrical vector E_o of polarized light with respect to the principal crystallographic axes a and c, are the matrix elements $M_{if}(\underline{k},h\omega)$ and $T(E,\underline{k})$ since the JDOS is a scalar determined entirely by the E vs k dispersion relations.

Furthermore, following reasons show that the polarization dependence on $T(E,\underline{k})$ would be a second or higher order correction only in the case of Sb_2Se_3.

(i) The electron-phonon interaction is isotropic in the (100) and (001) directions as demonstrated by the dc conductivity (†).

(ii) The electron-electron interaction (which is the strongest scattering at the high $\hbar\omega$) in the two directions is also almost isotropic as deduced from the "energy loss-function" $\mathrm{Im}\,\frac{1}{\varepsilon_1 + i\varepsilon_2}$ (2).

(iii) The strongly directional velocity of electrons as a result of polarized light excitation would progressively smear out after each collision.

Therefore t'.e only term which can explain the very strong anisotropy of the reflectance and photoemission spectra of Sb_2Se_3 are the dipole excitation matrix elements. The close relation between eqs. (3) and (4) shows that the optical transition strength $\omega^2\varepsilon_2$ is the most suitable optical function to be used for comparison with the EDCs.

EXPERIMENTAL

1) Photoemission apparatus and light source

The 240 MeV storage ring of synchrotron radiation at the Physical Science Laboratory of the University of Wisconsin was used as a continuum light source. The beam was focussed at the entrance slit of a monochromator optically equivalent to the McPherson 225 model. Upon reflection and dispersion at the grating the beam is focussed at the exit slit of the monochromator and then diverges again (f = 10.4). Therefore, an ellipsoidal mirror was used to refocus the light beam to a spot of approximately 1 mm in diameter which illuminated the sample. Even though the beam is naturally polarized in the median plane of the storage ring, some depolarization occurs after reflections at focussing mirrors and the grating. The polarization of the light illuminating the sample was approx. 80%.

A double cylindrical electrostatic mirror with a channeltron was used as an electron energy analyzer. This analyzer which is described in detail elsewhere (8) detects only electrons of certain velocity which originate at a given point in space; this focal point of the analyzer was adjusted to coincide with the focussed beam illuminating the sample. By moving the sample with respect to the focal point of the analyzer it was possible to select the best surface area of the sample, the criterion being that the ratio of the high energy end of EDCs to the low energy peak due to scattering be made maximum. For good cleavages and uniform films this was only a second order correction, however. Instead of changing

the potential difference between two concentrical cylinders of the analyzer, the sampling of the velocity of the electrons was done by sweeping a retarding or accelerating voltage between two concentric hemispheres located in the region between the electron source and the analyzer entrance. The main advantage was that the analyzer resolution was then independent of the electron energy. In our case the analyzer was set to pass 20 eV electrons and the resolution was 0.2 eV for all electron energies. This pass energy gave the most favorable condition for high transmittance of the analyzer while retaining good resolution. Digital processing of the signal at the output of the channeltron eliminated the thermal noise, and the only limitation was the shot noise of the channeltron and the statistical error which resulted in the necessity of longer counting times for hv > 20 eV where both the yield and the light intensity started to decrease

2. Sample preparation

Orthorhombic single crystals of Sb_2Se_3 (space group D_{2h}^{16}, a = 11.62Å, b = 11.77Å, c = 3.96Å) were grown from melt in a horizontal zone refiner by method described (9) from 6-9's purity elements. Samples approx. 9 x 9 x 3 mm were cut from ingots of approx. 1/2" diameter and 10" long. The base pressure in the photoemission chamber was 8 x 10^{-10} torr and did not change substantially during the cleaving. Excellent mirror-like cleaved surfaces $\perp$b were obtained which enabled the sample to be illuminated at $E_o||a$ or $E_o||c$, respectively. (E_o is the electric vector of polarized light).

Amorphous Sb_2Se_3 films of thickness ~200 to 500Å were prepared in situ by evaporation of Sb_2Se_3 from E-B gun at very small rates (approx. 1Å/sec) onto nickel and quartz substrates with Pt contact. This method of evaporation had been developed earlier (10) to produce amorphous stoichiometric Sb_2Se_3 films within the 1% error in composition detectable by an electron microprobe method. After the photoemission measurements the films were checked by X-ray diffraction and were indeed found to be amorphous. The pressure before the evaporation was 5 x 10^{-10} torr rising to a 4 x 10^{-9} torr during the evaporation and decreasing back to 8 x 10^{-10} torr immediately after the E-B gun was turned off.

EXPERIMENTAL RESULTS

The experimental data (EDCs) are presented at figs. 1-3 for both orientations of the electrical vector E_o of the polarized light $E_o||c$, $E_o||a$ and for amorphous Sb_2Se_3. It is seen that the EDCs exhibit the most sharp and most rich structure in the photon energy range between 7 eV and approx. 15 eV. At higher photon energies the structure (peaks, shoulders, valleys) is getting progressively less sharp as a result of the increasing contribution of scattered electrons which build a structureless background at the lower energy part of EDCs and decrease the signal at the high energy end. Starting at approx. 20 eV an additional overall decrease of the signal occurs as a result of decreasing efficiency of the normal incidence grating monochromator. Therefore primarily the 7 to 20 eV region of hν will be used for further analysis (11).

Since there is present a large amount of structure in our data as a result of strong polarization dependence, a large span of photon energy, and probably very complex band structure, it is advantageous to identify briefly the most prominent structure in Figs. 1-3. There are two sharp peaks A and B in crystalline Sb_2Se_3 and one broad peak AB in amorphous Sb_2Se_3 at the high energy end of EDCs for hν in the 8 eV to 30 eV range, and these are separated from the rest of the EDCs by a valley V approx. 2 eV from the high energy end of the EDCs; additional peaks C and D are located approx. 0.6 eV and 1.3 eV below the valley V for crystalline Sb_2Se_3. All the above structure has constant energy of the initial states. There are several shoulders and peaks P_0 to P_4 in crystalline

Sb_2Se_3 and one structure P in amorphous Sb_2Se_3 which indicate a constant final state energy. For further interpretation we will use the standard method of structure plots where the final energy E of each element of the structure is plotted vs the photon energy hν. Since the position of the Fermi level is rather uncertain due to the effect of the surface states and the field penetration, all energies will be referred to the top of valence band rather than to the Fermi level. The high (and energy independent) resolution of the analyzer used provides rather sharp leading edges of the EDCs which can be easily extrapolated to define the top of the valence band. The very weak tail at the high energy end of the EDCs is due to both intrinsic broadening (as a result of the electrical field penetration (6)) as well as to the instrumental broadening (nonuniform work function of the analyzer, nonmonochromatic light and the final resolution of the analyzer).

Crystalline Sb_2Se_3

$E_o||c$

In the region between the threshold energy and hv = 8.0 eV, a strong peak in EDCs occurs close to the top of the valence band (line α' in fig. 4). This structure which does not have the slope of the E = hv lines ends at hv = 8.0 eV and is attributed to direct transitions.

At hv = 8.0 eV there occurs a change in the overall structure of the EDCs (sharp peak associated with a very sharp shoulder in $\omega^2\varepsilon_2$) which shows up in fig. 4 as the onset of three new lines parallel with the E = hv line and corresponding to peaks A and B. This structure persists in the entire photon energy range and is separated from the remaining part of the EDCs by a valley V. The high resolution of our experiment shows that in the 8 eV to 15 eV region peak B is a doublet separated by approx. 0.3 eV. Since the two peaks A, B and the valley V occur in extremely large photon energy range over 20 eV with constant well defined initial energy, we conclude that they represent a large density of states in the valence band, arising from flat E vs k part of the band. In addition to the above structure there is noticeable also a weak shoulder at the leading part of the EDCs.

Fig. 4 shows several other structures γ and δ located 0.4 eV to 1.[illegible] eV below the valley V starting at approx. hv = 10 eV and corresponding to peaks C and D in the EDCs. These structures have different relative intensity in the 10.0 eV to 15 eV region and a slope generally different from the E = hv line; they are associated with direct transitions contributing to the two reflectivity and $\omega^2\varepsilon_2$ peaks at hv = 10 eV and 12.5 eV.

There is a suggestion of another deeper lying structure in the valence band (points F, G, H) obscured by the background of scattered electrons and by the conduction band structure.

Another feature in fig. 4 are the five horizontal lines P_0 to P_4 corresponding to constant final energy of states and therefore we associate them with larger density of states in the conduction band. Their energy levels measured from the top of the valence band are 9.5 eV, 8.5 eV, 7.7 eV, 7.2 eV and 6.5 eV, resp. It is interesting to note that at several crossings of this conduction band structures with the valence band structure strong peaks in EDCs occur, as demonstrated for example at the intersections of line P_1 with lines A and B as seen in the EDCs for hv = 9.1 and 10 eV, resp. This fact together with the polarization dependence of the relative intensity of peaks A and B indicates that these peaks in the EDCs are due to direct transitions enhanced by matrix elements and by the regions of high density of states in both bands.

$E_o||a$

The plot of the energy position of major structure (Fig. 5) is more simple than for the $E_o||c$ orientation. All structure but line α' ending at 7.9 eV follows either the E = hv line or retains constant energy of the final states indicating again the existence of higher densities of states in both bands.

At the vicinity of hv = 8.0 eV there occurs also a change in the overall character of the EDCs, but this change is not reflected so strongly in the structure plot at for the $E_o||c$ case and the very sharp shoulder in $\omega^2\varepsilon_2$ for $E_o||c$ is now missing. One can just see a rather continuous onset of lines α, β and later γ and δ corresponding to peaks A and B separated by valley V from peaks C and D. These four peaks A, B, C and D are attributed to higher densities of states in the top part of the valence band, reflecting again flat E vs k portions of the valence band.

In addition to the above structure there exists again an indication of structure (points F, G, H) in the lower part of the valence band and an overall increase of density of states starting at 6 eV below the top valence band obscured by the conduction band structure and the background of scattered electrons. Due to the natural limitation of the photoemission experiment by the work function it is not possible to determine directly whether this deeper valence band starts to contribute to the reflectivity rise at approx. 7 eV.

Similarly to $E_o||c$, a series of five horizontal lines again shows the presence of a higher density of states in the conduction band at

levels 3.5 eV, 8.5 eV, 7.7 eV, 7.2 eV and 6.5 eV above the top of the valence band.

While the reflectivity and the optical transition strength $\omega^2\varepsilon_2$ exhibit the same two peaks at approx. 10 eV and 12.5 eV for both polarization, our EDCs clearly indicate that EDJDOS (the energy distribution of JDOS) is quite different for these two polarizations. The reflectivity peak at ~10 eV has strong contribution from peak A in EDCs for $E_o||a$ and from peak B for $E_o||c$. The reflectivity peak at ~12.5 eV has large contribution from peaks B and C in EDCs for $E_o||a$, and approximately equal from A and B for $E_o||c$. It is primarily the upper 3 eV of the valence band which provides strong polarization dependence to the EDJDOS which is not detectable in the optical data (e.g., for $E_o||a$ the very sharp peak A at 10 eV is changing into a very weak shoulder in the 11.5 eV to 15 eV region (†)). Since the EDCs represent the quantity $M^2 \quad N_v(E - h\nu)$ $N_c(E) \quad T(E)$ where N_v, N_c and $T(E)$ are scalars, this strong polarization dependence of the relative strength of peaks A and B in the 8 to 15 eV region reveals a strong dependence on matrix elements. This shows that even though peaks A, B are arising from flat E vs k band portions of the valence (which implies higher density of states), the transitions are however still direct, i.e., the $\vec{k}$ vector conservation is still important selection rule and the constant matrix element approximation cannot be used. These transitions from the flat portions of the upper valence band being further either enhanced or forbidden by matrix elements and by high conduction band density of states (P_0 to P_4) make a considerable contribution to the reflectivity structure in the 8 to 15 eV region for both polarizations. This does not preclude another group

of transitions from deeper valence bands whose onset however cannot be determined from this experiment due to the work function limitation. This strong polarization dependence of the EDCs clearly demonstrates the necessity of using polarized light for photoemission studies of noncubic solids. Inspection of our EDCs for $E_o||c$ and $E_o||a$ shows that most of the structure including peaks A, B and C would be lost or strongly suppressed if a nonpolarized light were used in the 8 to 15 eV region.

Amorphous Sb_2Se_3

The total photoemission yield of amorphous Sb_2Se_3 films was several times lower than that of crystalline Sb_2Se_3, and the low energy part of the EDCs was partially obscured by the background of photoelectrons emitted from the analyzer (12). The correction for this effect at several photon energies is shown in fig. 3 (dashed line). These corrected EDCs still include, however, the secondary and scattered electrons originating in the conduction band of Sb_2Se_3 films.

The structure of the EDCs for amorphous Sb_2Se_3 is much less complicated than for crystalline, yet the main features are still similar. There are again a shoulder S and a peak AB at the high energy end separated from the rest of the EDCs by the valley V. However the two very sharp peaks A and B in crystalline Sb_2Se_3 forming this broad peak AB are now very diffuse and the peaks C and D at the low energy side of V are completely missing. Amorphous Sb_2Se_3 also does not exhibit the change in the structure plot at $h\nu \approx 8$ eV. Both peak AB and the valley V indicate again the constant initial energy of states attributed primarily to the valence band structure, and their behavior in fig. 6 exhibits typical features of nondirect transitions. The lower part of the valence band (points F, G, H) is resolved even sharper in amorphous than crystalline Sb_2Se_3 despite lower yield in case of films, the reason being probably much weaker conduction band structure in amorphous Sb_2Se_3. There is seen just one region D of higher density of states in the conduction band at 7.7 eV above the top of the valence band corresponding to P_y in crystalline Sb_2Se_3. It is interesting to note that due to the high resolution

(0.2 eV) of our apparatus both crystalline and amorphous Sb_2Se_3 exhibit very sharp high energy ends of the EDCs, particularly there is no direct evidence of the density of states tailing in the amorphous stochiometric Sb_2Se_3. This is in agreement with previous findings from the optical and photoconductivity data (13) (14), which was explained by the strong suppression of the matrix elements for transitions from localized to extended states.

DISCUSSION

One important feature of the EDCs is the strong structure in the upper 2 eV part of the valence band. In case of crystalline Sb_2Se_3 this region is clearly split (peaks A and B) and indicates two flat E vs k portions of the valence band. Even though the behavior of peaks A and B itself in graphs 4 and 5 does not allow a choice between indirect transitions and direct transitions from flat bands, the polarization dependence of relative intensity of peaks A and B shows that the latter is the case since the only polarization dependent term in EDJDOS are the matrix elements $M(\omega, \vec{k})$. This region of the upper 2 eV in the valence band undergoes a large change at the transition from crystalline to amorphous phase. Peaks A and B merge into one broad peak AB in amorphous Sb_2Se_3 which does not allow for a very flat E vs $\vec{k}$ band and its behavior in Fig. 6 shows that it is due to nondirect transitions with constant matrix elements. (The width and energy position of the AB peak also suggests it could originate from overlapping the two wave functions responsible for two sharp peaks A and B in crystalline Sb_2Se_3.) An additional confirmation on the role of the $\vec{k}$ conservation and of matrix elements comes from comparison of the optical transition strength $\omega^2\varepsilon_2$ for amorphous and crystalline Sb_2Se_3. Even though the upper 2 eV part of the valence band has the overall general structure for both phases, there occurs a sharp peak in $\omega^2\varepsilon_2$ at $h\nu \sim 3$ eV for both polarizations as a result of matrix element enhancement while it is completely missing in amorphous Sb_2Se_3. This cannot be explained in terms of the lowest conduction band structure only since the $\omega^2\varepsilon_2$ spectra are polarization dependent.

The other portion of the valence band being strongly affected by the phase transition is located approx. between 2.0 and 3.3 eV below the band top (peaks C and D). Again there is strong polarization dependent enhancement in the hv = 9 to 15 eV region as a result of matrix elements in crystalline Sb_2Se_3, and fig. 5 clearly shows the transitions from peaks C and D to be direct. On the other hand the lower portion of the valence band starting at approx. 4 eV below the top (points F, G, H) does not exhibit strong dependence on the polarization or phase transition and is even better seen in the amorphous film due to weaker conduction band structure. Of particular interest is an additional increase of the density of states starting 6 eV deep in the valence band which is seen in figs. 2, 3 and 4 for curves at hv > 17.5 eV. In the region hv > 17 eV there is little overlapping of the valence and conduction band densities of states, and the upper part of the EDCs can be then thought with reasonable accuracy as the replica of the valence band density of states (yet superimposed on smooth background of scattered electrons and of density of states of s-like conduction band). This is further supported by the X-ray photoemission data on Sb_2Se_3 (15). It is conceivable to assume that this lower portion of the valence band contributes significantly to the reflectivity rise at hv = 7 eV even though the onset of these transitions cannot be seen at our EDCs due to the work function limitation which does not allow us to sample the lowest 5 eV of the conduction band.

The conduction band shows five closely spaced density of state structures between 6.5 and 9.5 eV (P_0 to P_4) for both polarizations in crystalline Sb_2Se_3 and a structure P at about 7.7 eV for amorphous Sb_2Se_3. Since these structures occur in the low energy part of EDC there might be a

possibility that these high density of states in the conduction band are filled rather by scattering of hot electrons in the conduction band than by optical excitation. This possibility is ruled out, however, by the appearance of strong peaks in EDCs at the crossing of the conduction and valence bands densities of states which suggests interband optical transitions. In addition, we did not interpret any possible structure occurring in the lowest 1 eV region of EDCs to eliminate possible effects due to the modulation of the density of states by the escape function. Therefore, all structure presented in figs. 4-6 is due to optical transitions.

Since there have been no band structure calculation for Sb_2Se_3 or similar orthorhombic V-VI compounds (primarily due to its very complicated primitive cell containing 112 valence electrons), the only theoretical model for the electronic structure of Sb_2Se_3 is the valence band approach (16) (17). Our results can be then interpreted in general terms of bonding orbitals in the following way. The upper part (first 6 eV) of the valence band is attributed to "nonbonding" or weakly-bonding states arising either from unpaired bonds (like the two p-electrons of sulfur in isostructural Sb_2S_3) or from pivotal resonance arising from hybridized sp_zd_z orbitals. The latter have been found very strongly affected by the change in the long range order (18), and the peaks A, B, C and D in our EDCs also show the strongest dependence on the long range order. The lower part (6 eV or more) of the valence band which does not depend strongly on the long range order is attributed to bonding states which are effected primarily by the short range order only.

The conduction band structure suggested by our EDCs is a smooth s-like band with superimposed flat bands at the 6 to 10 eV region. The

bonding orbital model supposing filled valence shell of Se provides indeed an explanation of these higher densities in conduction band as arising from some 5p states of Sb and the additional spd hybridizing orbitals superimposed on smooth s-like band (probably Sb 6s). These hybridized orbitals are then further split by the crystal field into several levels. Several of these conduction band higher densities of states are directly coupled with the valence band in optical excitations and are believed to make a considerable contribution to the reflectivity and $\omega^2\epsilon_2$ peak at $h\nu = 10$ eV for both amorphous and crystalline Sb_2Se_3.

CONCLUSION

The presented EDCs show high density of states in the upper 3 eV of the valence band which in the case of crystalline Sb_2Se_3 are arising from very flat portions of E vs k bands, and in terms of bonding orbitals can be assigned to resonance orbitals (either the unpaired p electrons or the pivotal resonance). The optical transitions from these states are strongly polarization dependent and are direct (i.e., $\vec{k}$ conserving) in crystalline Sb_2Se_3. These states are the most strongly affected at the transition into amorphous phase as demonstrated by the merging of A and B into one broad peak AB, disappearance of peaks C and D, and by waiving the $\vec{k}$ vector conservation (i.e., nondirect transitions instead of direct occur). The last point is in agreement with the reflectance spectra and the $\omega^2\varepsilon_2$ spectrum in the 0 to 6 eV region (2). The next lower 3 eV part of the valence band (F, G, H) is obscured by the conduction band structure and scattered electrons; the density of states is decreasing at approx. 5 eV below the top of the valence band for both phases. A new polarization independent region of high density of states in the valence band starts about 6 eV from the top for both phases which we attribute to bonding orbitals. The high conduction band density of states arising possibly from hybridized spd orbitals were found in the 6.5 to 9.5 eV region for crystalline and at 7.7 eV for the amorphous Sb_2Se_3.

The EDCs show that the far UV reflectance spectra of Sb_2Se_3 can be explained in terms of the JDOS (i.e., including also the high density of states in the conduction band) and of matrix elements rather than by the

simplified model of bonding and nonbonding valence band (4). Particularly the reflectivity peaks at 10 eV and 12 eV have still very strong contribution from transitions between the upper 3 eV region of the valence band and the high densities in the conduction band which are in case of crystalline Sb_2Se_3 strongly polarization dependent and further enhanced by matrix elements as shown by EDCs. However, this matrix elementdependence is not detectable in the 4 to 15 eV region by the optical methods due to their integral nature when compared to the differential nature of the photoemission method.

ACKNOWLEDGEMENTS

We thank the staff of the University of Wisconsin Physical Science Laboratory for their valuable help and assistance during the measurements, B. Van Pelt for growing the Sb_2Se_3 crystals and help with cleaving the crystals, and R. Mueller for performing the X-ray diffraction. We also thank Dr. J. C. Shaffer for many valuable discussions and Dr. F. M. Mueller for critical reading of this manuscript.

REFERENCES

1. S. D. Shutov, V. V. Sobolov, Y. V. Popov and S. N. Shestatskii, Phys. Stat. Sol. 31, K23 (1969).

2. J. C. Shaffer, B. Van Pelt, C. Wood, J. Freeouf, K. Murase and J. W. Osmun, to be published.

3. R. Zallen, R. E. Drews, R. L. Emerald and M. L. Slade, Phys. Rev. Lett. 26, 1564 (1971).

4. R. E. Drews, R. L. Emerald, M. L. Slade and R. Zallen, Solid St. Comm. 16, 293 (1972).

5. K. Murase, J. W. Osmun, J. Freeouf, M. Kastner and C. Wood, Bull. APS 17 (2), 345 (1972).

6. R. C. Eden, Ph.D. Dissertation, Stanford University, 1967 (unpublished).

7. W. F. Krollikowski, Ph.D. Dissertation, Stanford University, 1967 (unpublished).

8.

9. C. Wood, B. Van Pelt and E. Hyland, Rev. Sci. Inst. (in press).

10. R. Mueller and C. Wood, J. Non-Cryst. Solids (in press).

11. The EDCs for $h\nu \geq 20$ eV look similar to those for 20 eV but the structure is even weaker. The main purpose of taking the EDCs for $h\nu > 20$ eV was to obtain information on possible contribution from core d-levels (the 4d level of Sb). Our results show no core d-bands in the 7 to 40 eV region which indicates that the optical properties of Sb_2Se_3 in ref. 2 are due to the s and p valence electrons only.

12. Even though the analyzer used detects only the electrons originating at its focal point, it is not able to discriminate against electrons emitted from other parts of space yet having a virtual origin at its focal point. Most of the background electrons come from the mesh used in the light port to prevent fringe fields inside the analyzer.

13. C. Wood, Z. Hurych and J. C. Shaffer, Proc. of 4th Int. Conference on Amorphous and Liquid Semiconductors, Ann Arbor, Michigan, 1971 J. Non-Cryst. Solids (in press).

14. Z. Hurych, R. Mueller, C. C. Wang and C. Wood, J. Non-Cryst. Solids (in press).

15. C. Wood, J. C. Shaffer and W. G. Proctor, to be published.

16. E. Mooser and W. B. Pearson, Progress in Semiconductors 5 104 (1960).

17. E. Mooser and W. B. Pearson, J. Phys. Chem. Solids, 7, 65 (1958).

18. A. S. Karpus and I. V. Batarunas, Chem. Bonds in Semicond., edited by N. N. Sirota, p. 203, Consulat Bureau, New York, 1967.

CAPTIONS TO FIGURES

Figure 1: Unnormalized photoelectron energy distribution curves (EDCs) for crystalline Sb_2Se_3 at $E_o||c$.

Figure 2: Unnormalized photoelectron energy distribution curves (EDCs) for crystalline Sb_2Se_3 at $E_o||a$.

Figure 3: Unnormalized photoelectron energy distribution curves (EDCs) for amorphous Sb_2Se_3. (Dashed curves are corrected for the analyzer background).

Figure 4: Structure plot for crystalline Sb_2Se_3 at $E_o||c$.

Figure 5: Structure plot for crystalline Sb_2Se_3 at $E_o||a$.

Figure 6: Structure plot for amorphous Sb_2Se_3.

FOOTNOTE

(†) It is possible that this weak shoulder is due to the nonpolarized component (approx. 20%) of the radiation and that it would disappear if 100% polarized radiation were used. (B. Van Pelt, private communication)

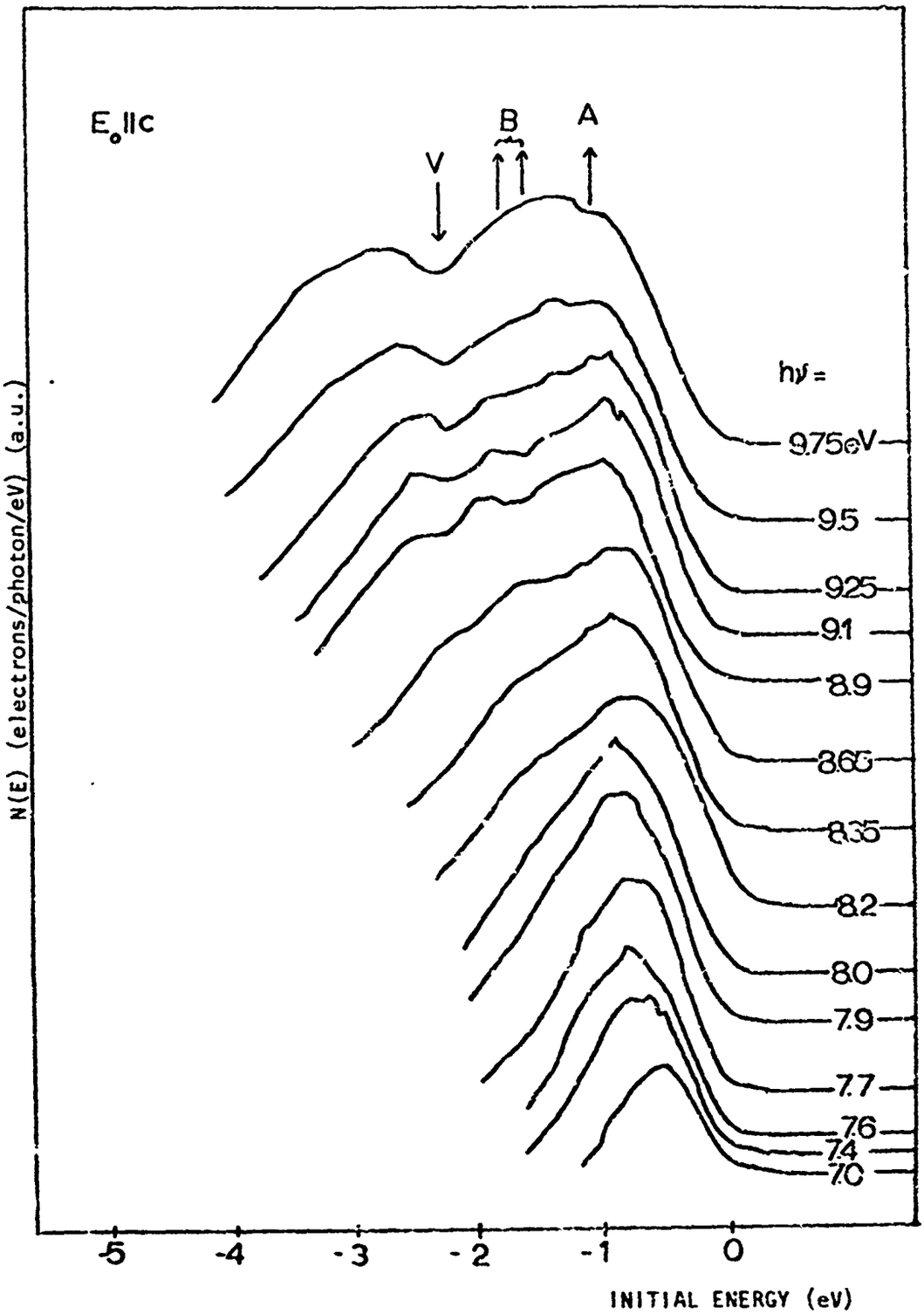
E₀⊥c
V
B
A
hν =
9.75eV
9.5
9.25
9.1
8.9
8.65
8.35
8.2
8.0
7.9
7.7
7.6
7.4
7.0
N(E) (electrons/photon/eV) (a.u.)
-5
-4
-3
-2
-1
0
INITIAL ENERGY (eV)

Fig. 1a

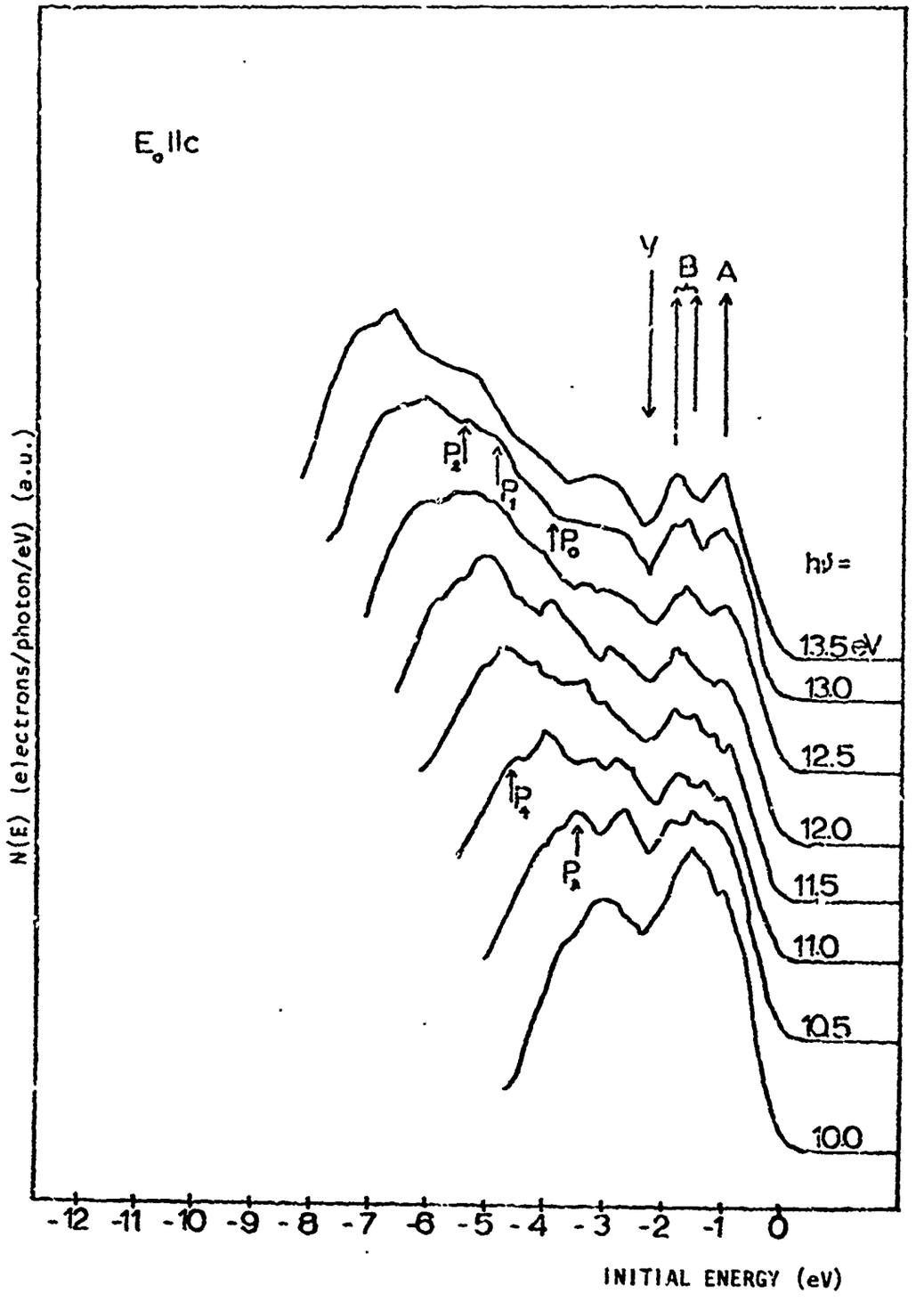
E₀ ∥ c
V
B
A
P₂
P₁
P₀
P₃
P₄
hν =
13.5 eV
13.0
12.5
12.0
11.5
11.0
10.5
10.0
N(E) (electrons/photon/eV) (a.u.)
-12 -11 -10 -9 -8 -7 -6 -5 -4 -3 -2 -1 0
INITIAL ENERGY (eV)

Fig. 1b

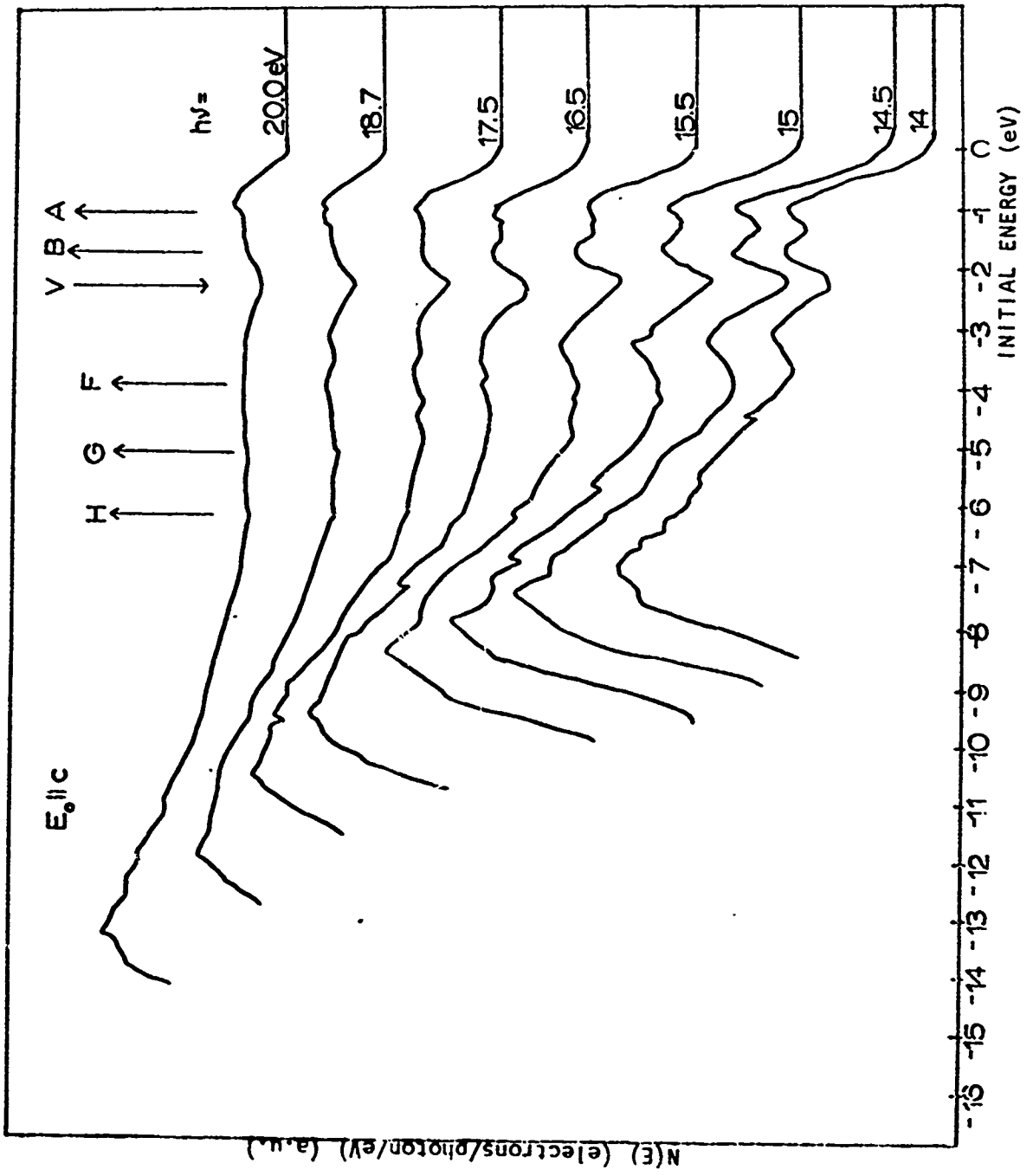
$E_o \| c$
H
G
F
V
B
A
hν=
20.0eV
18.7
17.5
16.5
15.5
15
14.5
14
-13 -15 -14 -13 -12 -11 -10 -9 -8 -7 -6 -5 -4 -3 -2 -1 0
INITIAL ENERGY (eV)
N(E) (electrons/photon/eV) (a.u.)

Fig. 1c

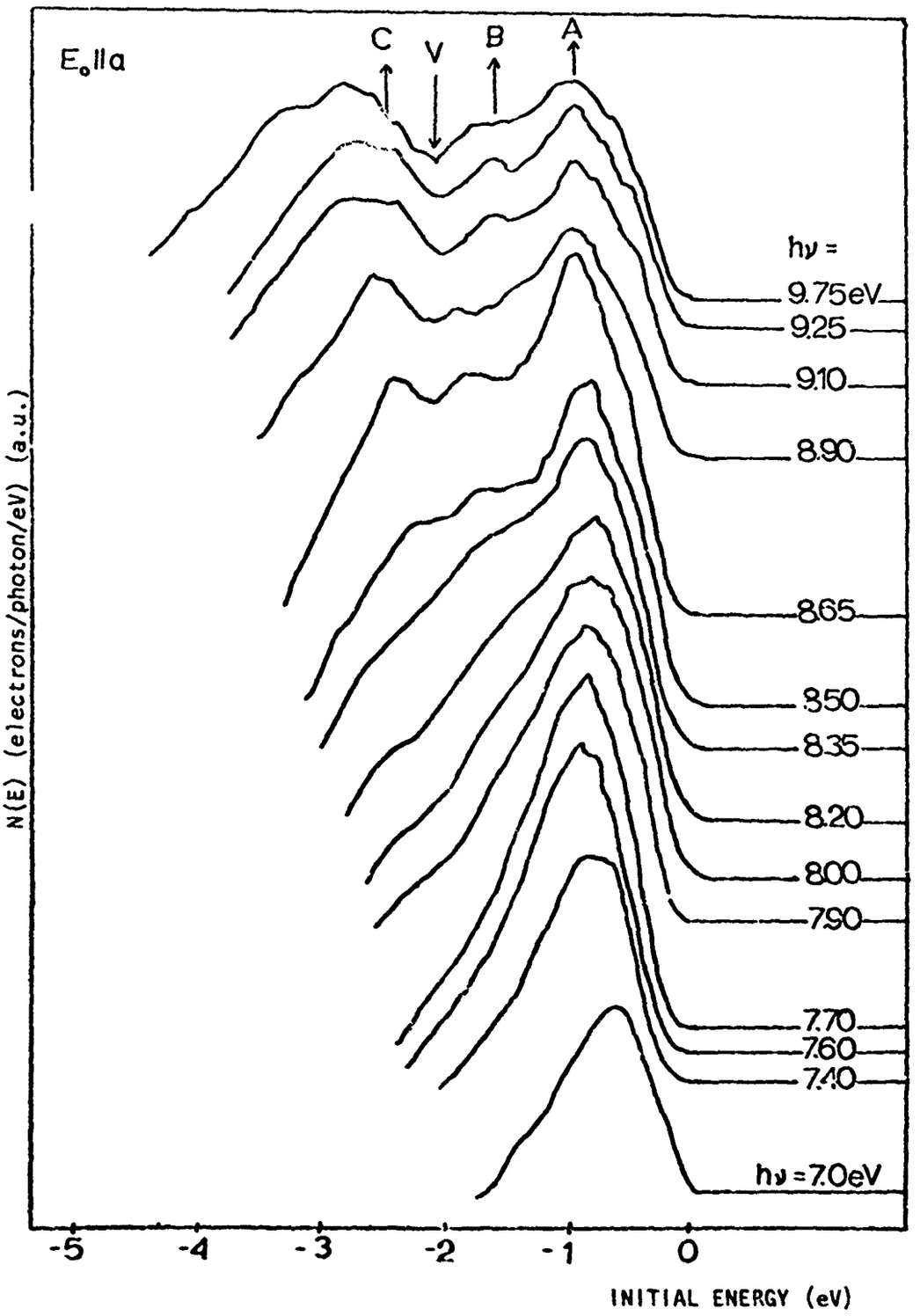
E₀∥a
C
V
B
A
hν =
9.75eV
9.25
9.10
8.90
8.65
8.50
8.35
8.20
8.00
7.90
7.70
7.60
7.40
hν = 7.0eV
N(E) (electrons/photon/eV) (a.u.)
-5
-4
-3
-2
-1
0
INITIAL ENERGY (eV)

Fig. 2a

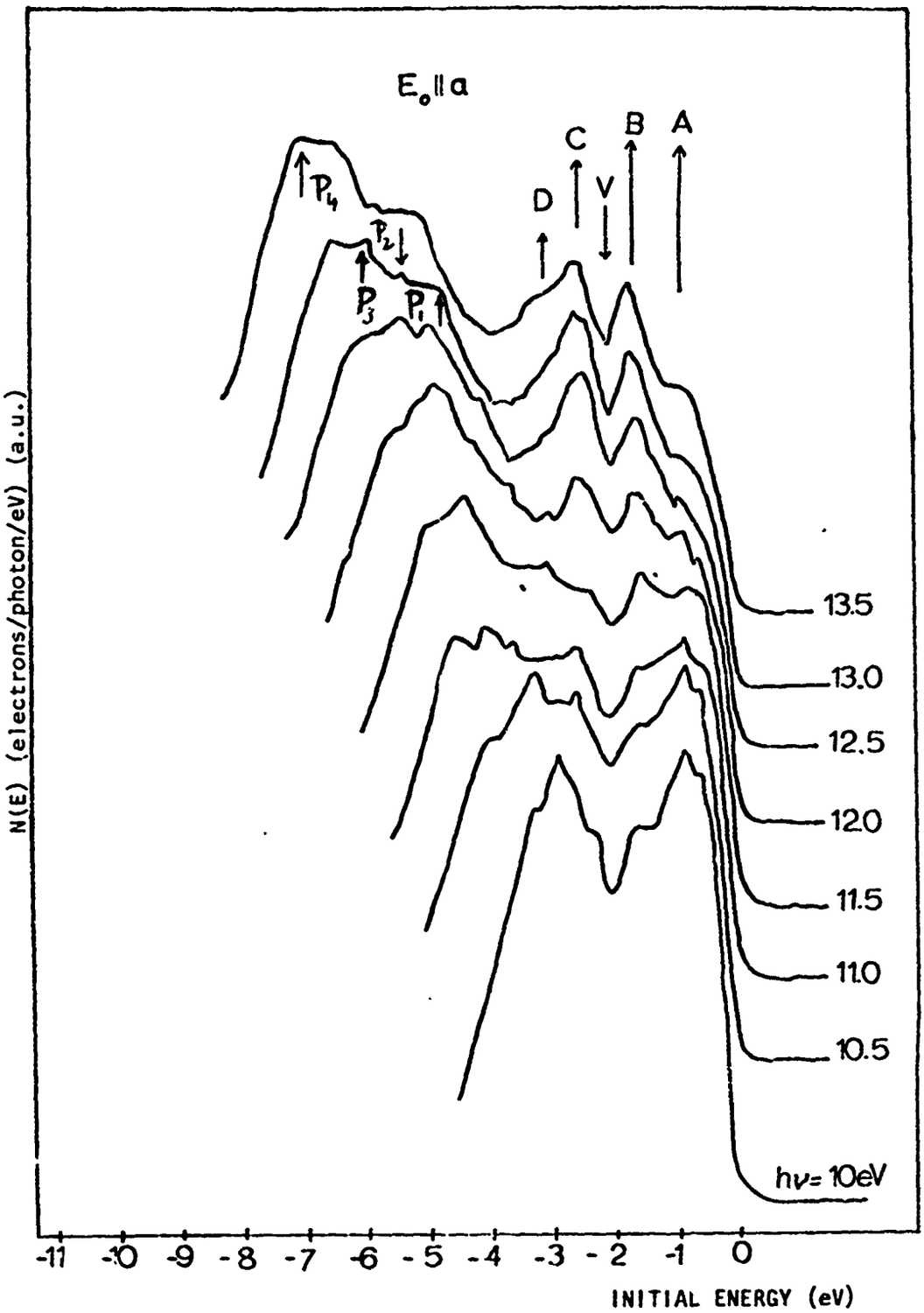
E₀∥a
A
B
C
D
V
P₁
P₂
P₃
P₄
13.5
13.0
12.5
12.0
11.5
11.0
10.5
hν= 10eV
N(E) (electrons/photon/eV) (a.u.)
-11 -10 -9 -8 -7 -6 -5 -4 -3 -2 -1 0
INITIAL ENERGY (eV)

Fig. 2b

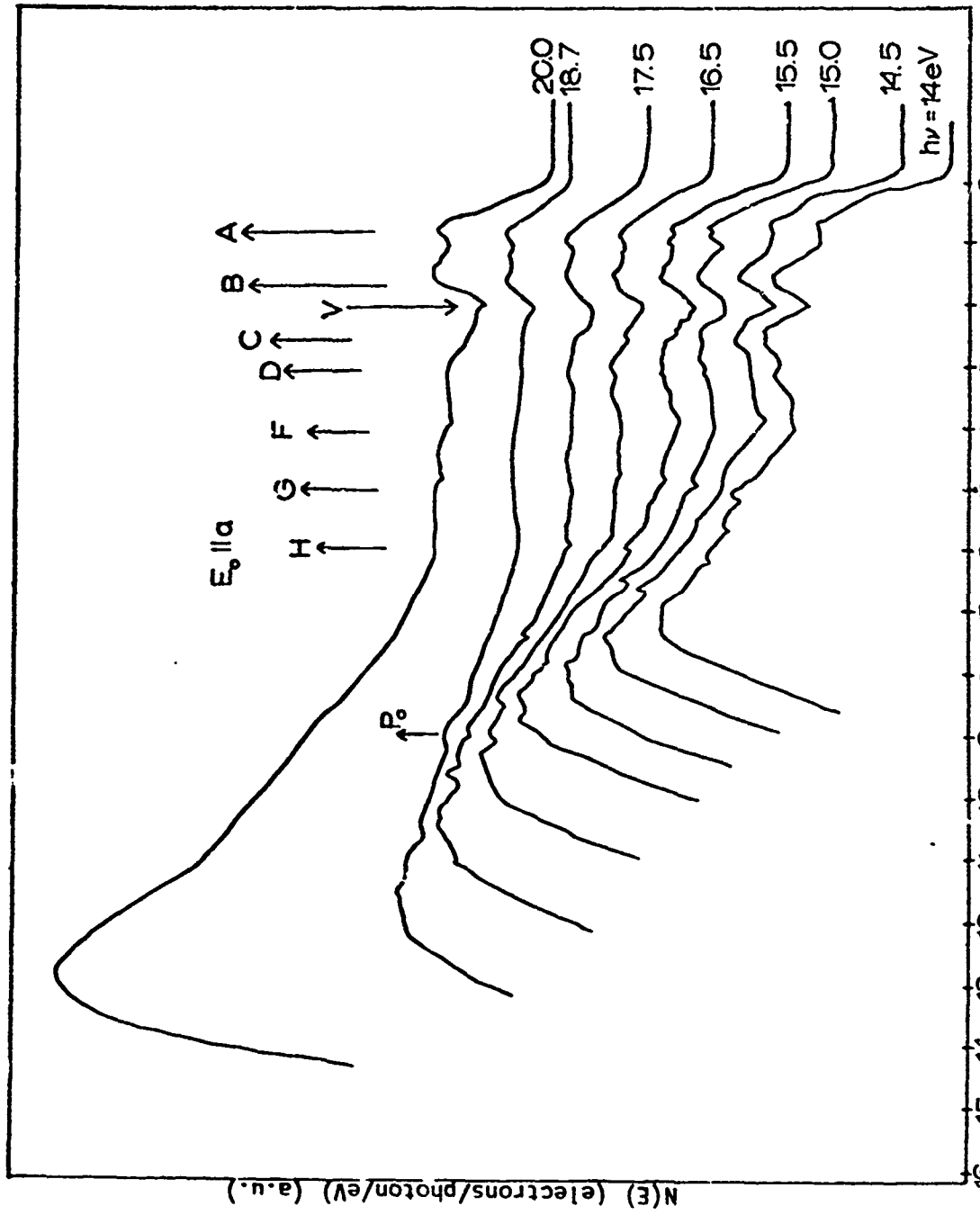
N(E) (electrons/photon/eV) (a.u.)
INITIAL ENERGY (eV)
0 -1 -2 -3 -4 -5 -6 -7 -8 -9 -10 -11 -12 -13 -14 -15 -16
hν=14eV
14.5
15.0
15.5
16.5
17.5
18.7
20.0
A
B
C
D
V
F
G
H
P°
E° ⊥a

Fig. 2c

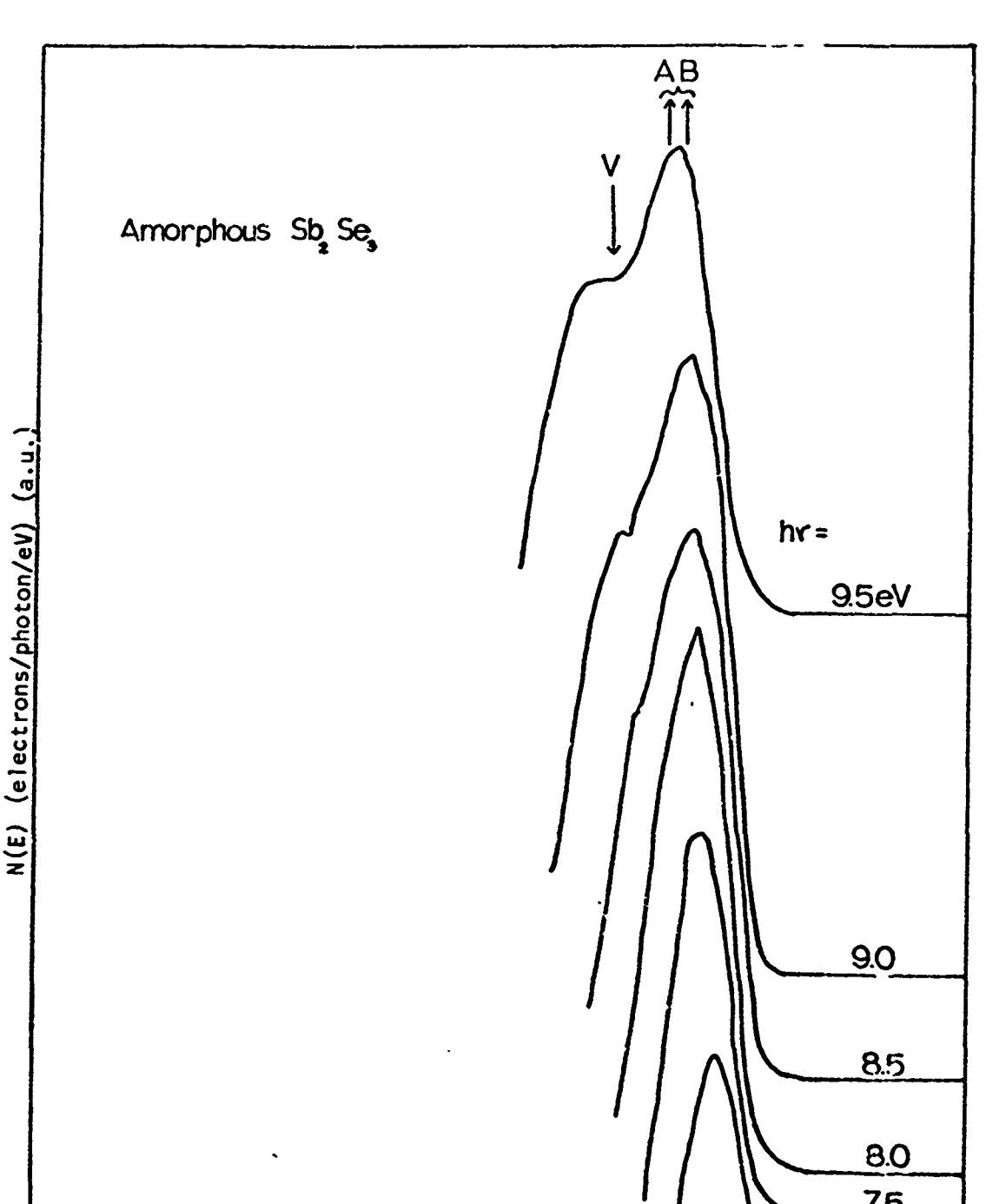
AB
V
Amorphous Sb_2Se_3
hr =
9.5eV
9.0
8.5
8.0
7.5
7.0
N(E) (electrons/photon/eV) (a.u.)
-12 -11 -10 -9 -8 -7 -6 -5 -4 -3 -2 -1 0
INITIAL ENERGY (eV)

Fig. 3a

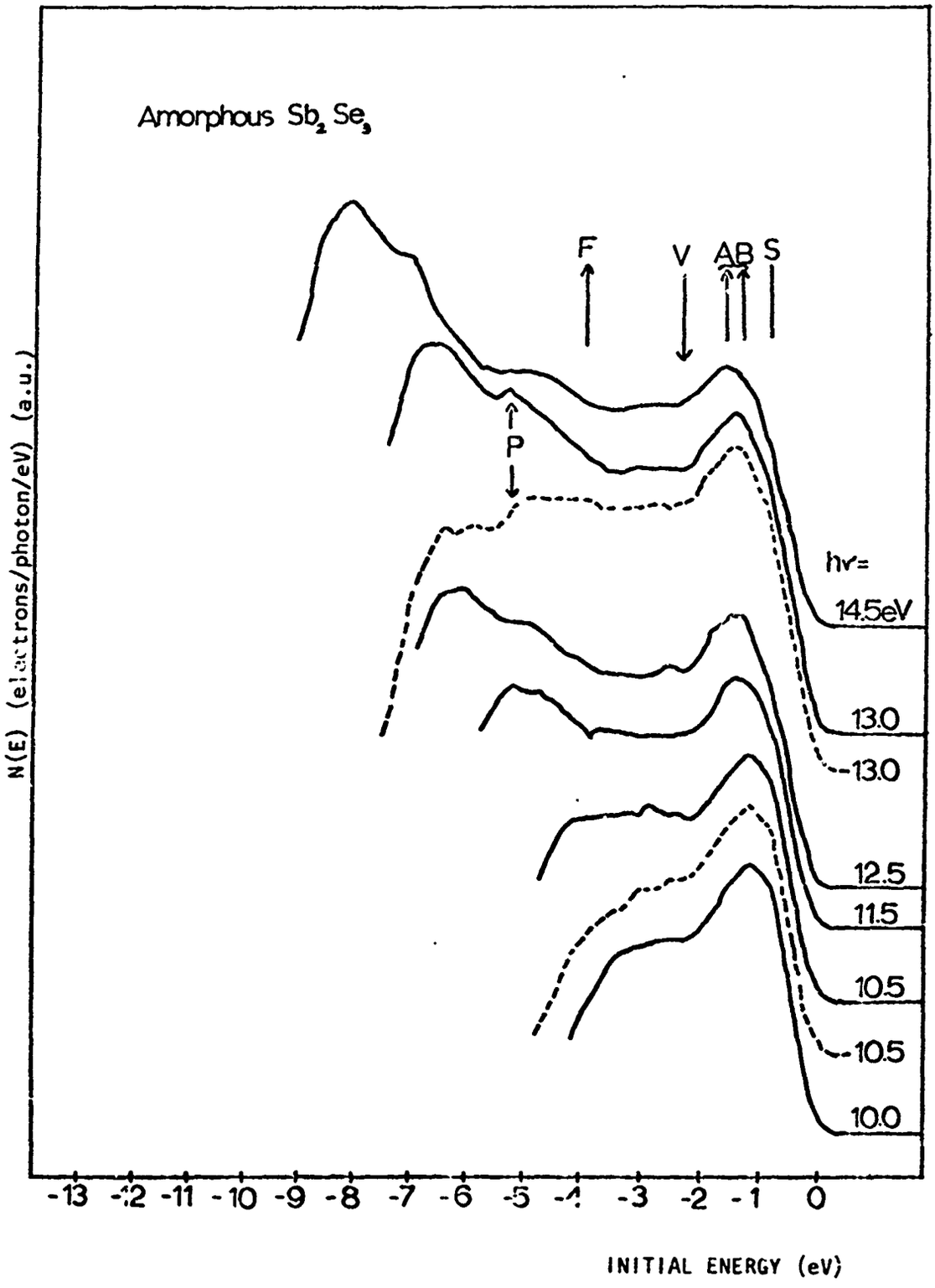
Amorphous Sb_2Se_3
F
V
AB
S
P
hν=
14.5eV
13.0
13.0
12.5
11.5
10.5
10.5
10.0
N(E) (electrons/photon/eV) (a.u.)
-13 -12 -11 -10 -9 -8 -7 -6 -5 -4 -3 -2 -1 0
INITIAL ENERGY (eV)

Fig. 3b

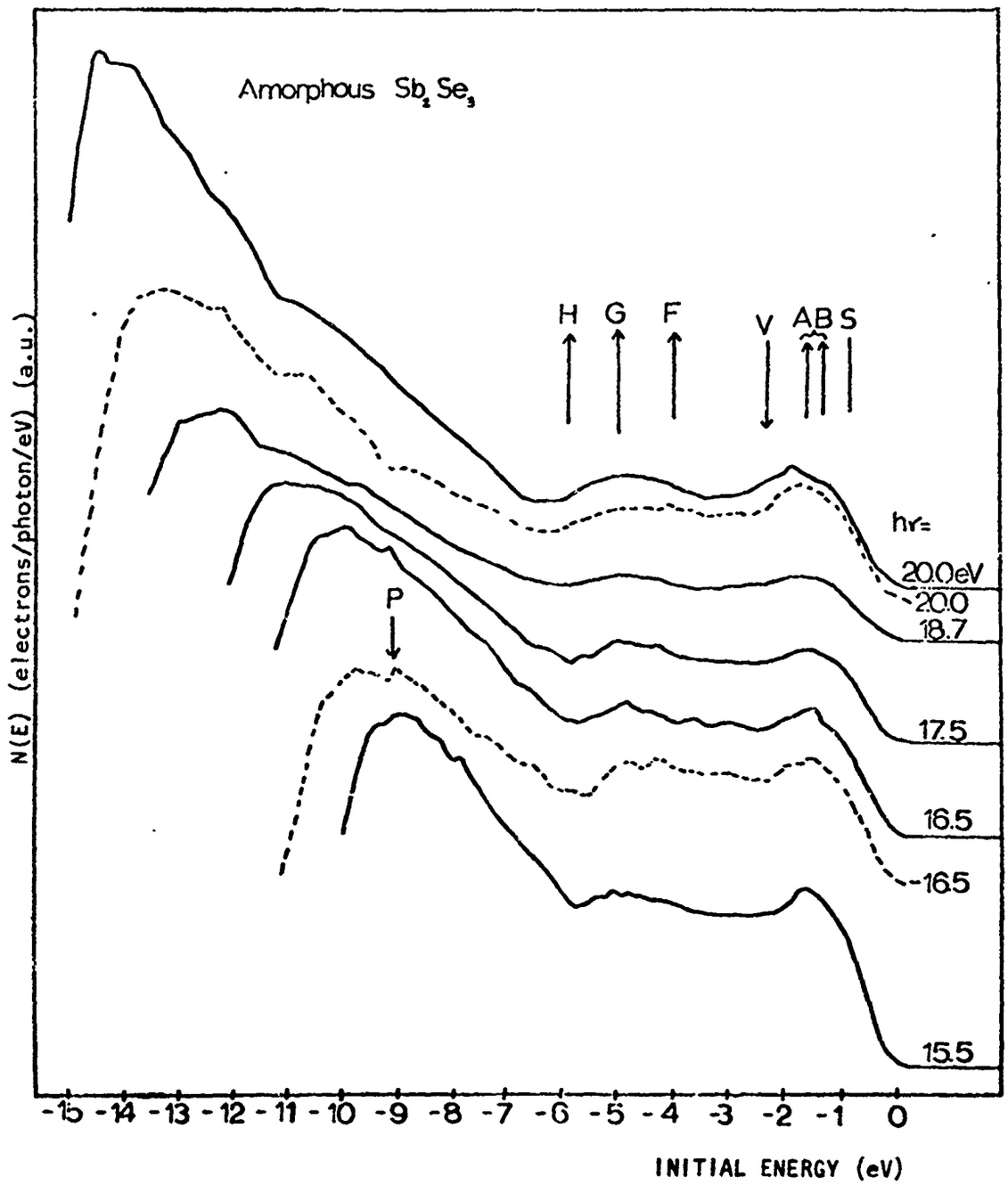
Amorphous Sb_2Se_3
H
G
F
V
AB
S
P
hr=
20.0eV
20.0
18.7
17.5
16.5
16.5
15.5
N(E) (electrons/photon/eV) (a.u.)
-15 -14 -13 -12 -11 -10 -9 -8 -7 -6 -5 -4 -3 -2 -1 0
INITIAL ENERGY (eV)

Fig. 3c

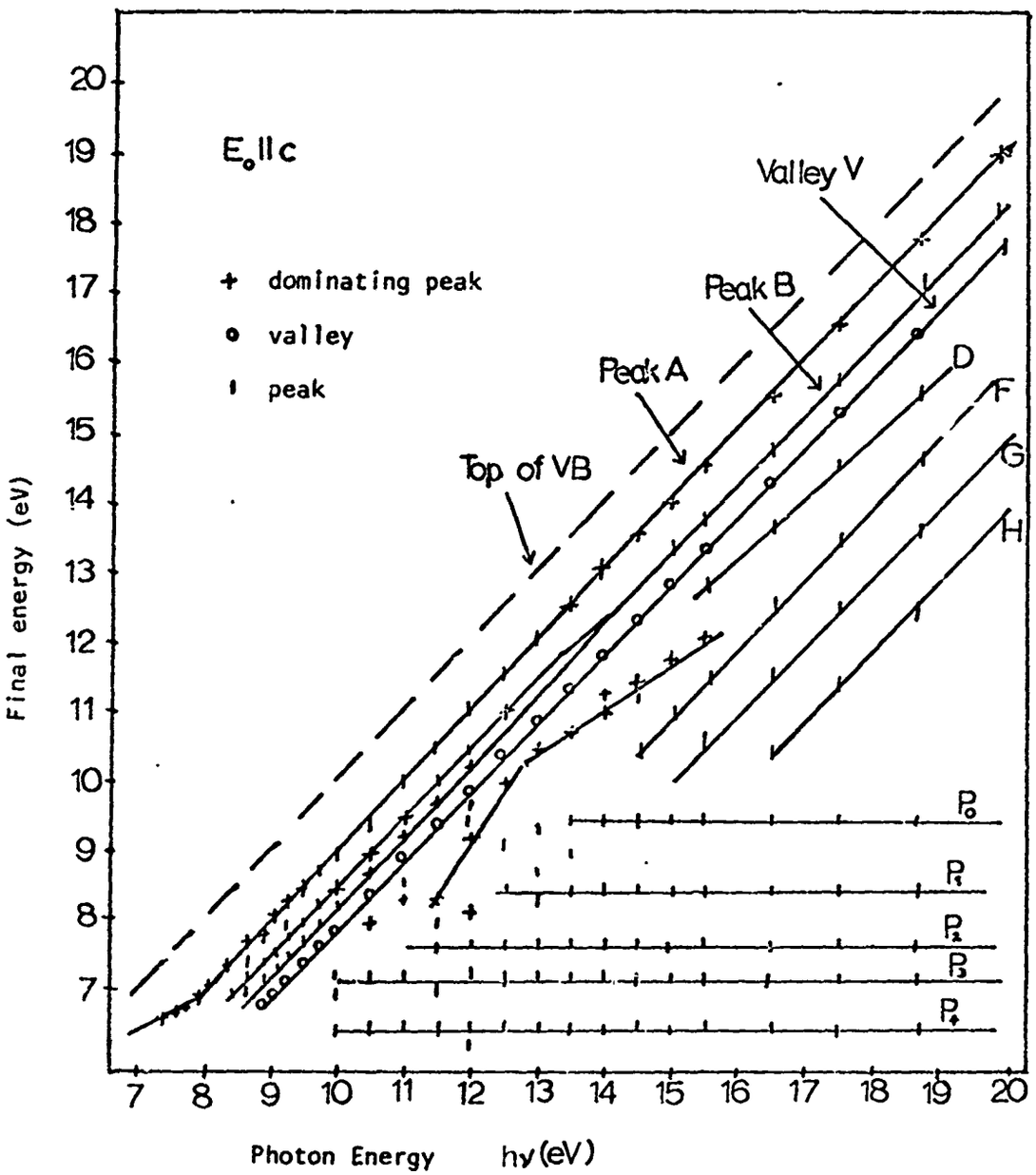
E_o llc
dominating peak
valley
peak
Valley V
Peak B
Peak A
Top of VB
D
F
G
H
P_0
P_1
P_2
P_3
P_4
Final energy (eV)
Photon Energy hν(eV)
20
19
18
17
16
15
14
13
12
11
10
9
8
7
7 8 9 10 11 12 13 14 15 16 17 18 19 20

Fig. 4

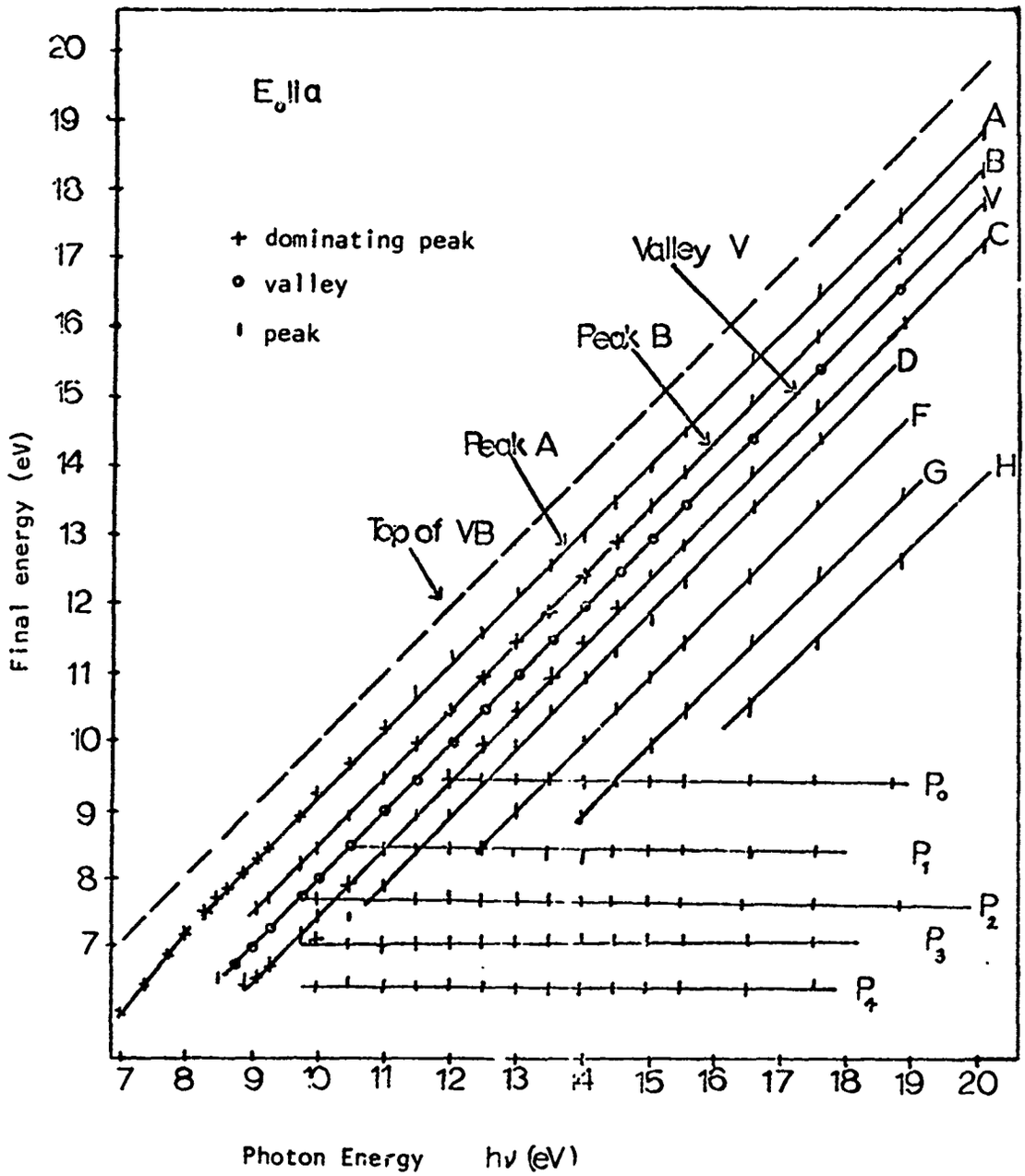
E₀⊥a
+ dominating peak
o valley
| peak
Valley V
Peak B
Peak A
Top of VB
A
B
V
C
D
F
G
H
P₀
P₁
P₂
P₃
P₄
Final energy (eV)
Photon Energy hν (eV)
20
19
18
17
16
15
14
13
12
11
10
9
8
7
7 8 9 10 11 12 13 14 15 16 17 18 19 20

Fig. 5

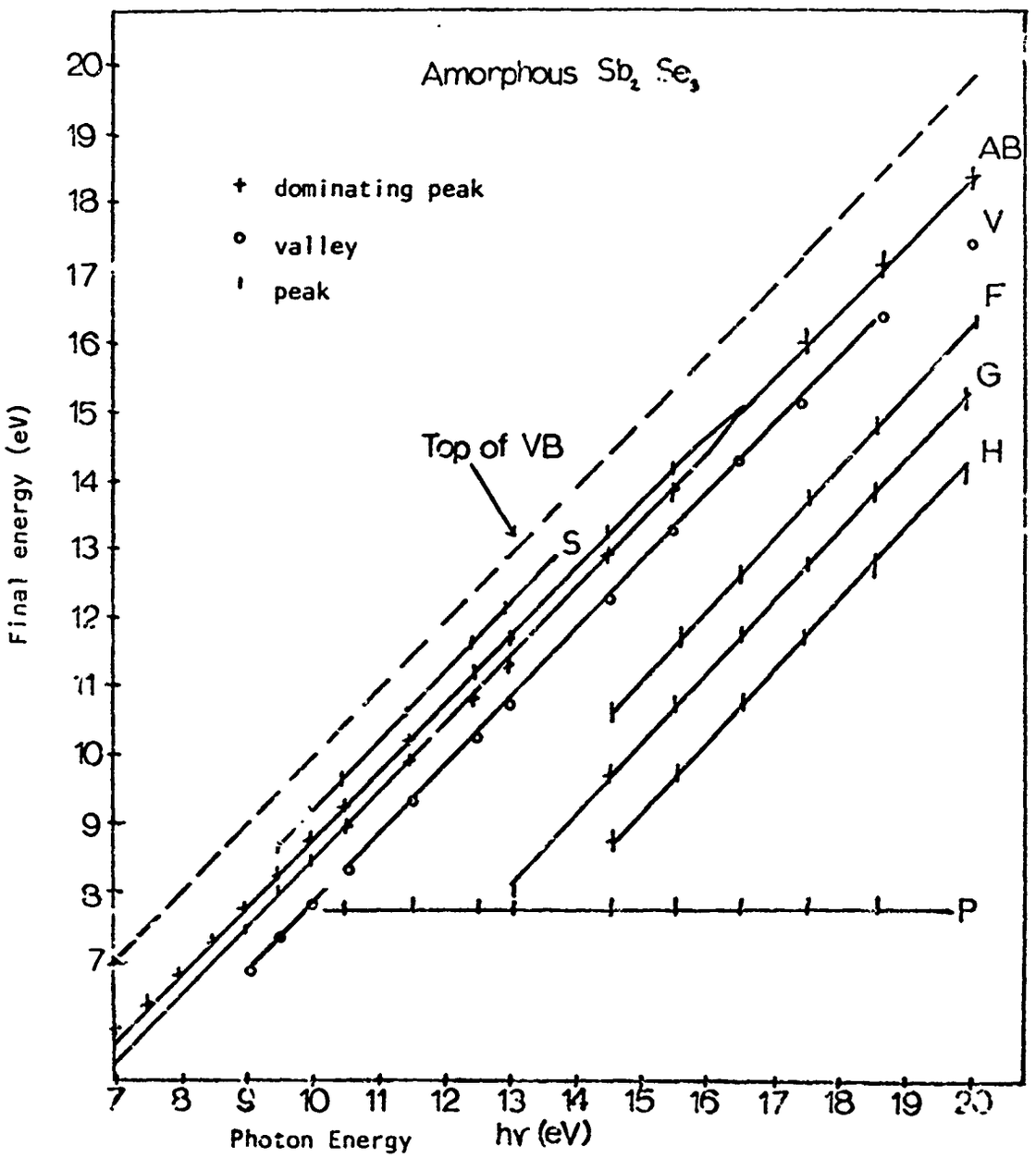
Amorphous Sb_2Se_3
+ dominating peak
o valley
| peak
Top of VB
AB
V
F
G
H
S
P
Final energy (eV)
Photon Energy hν (eV)
20
19
18
17
16
15
14
13
12
11
10
9
8
7
7 8 9 10 11 12 13 14 15 16 17 18 19 20

Fig. 6

APPENDIX C

ABSTRACT

The transition strength $(h\nu)^2\epsilon_2$ computed by Kramers-Kronig analysis of optical reflectance spectra is compared with X-ray photoelectron spectra (ESCA) for both single-crystal and amorphous Sb_2Se_3. The similarity of ESCA data for the two modifications suggests that the valence band structure is essentially the same whereas differences in the spectral dependence of $(h\nu)^2\epsilon_2$ suggest that the conduction band density of states is lower in the amorphous material, or that the matrix elements for optical transitions are suppressed.

Electron Energy States in Sb_2Se_3†

C. Wood and J. C. Shaffer
Physics Department
Northern Illinois University
DeKalb, Illinois 60115

and

W. G. Proctor
Instrument Division
Varian Associates
Palo Alto, California 94303

As part of a study of the optical properties of Sb_2Se_3 we have compared the energy dependence of the transition strength $(h\nu)^2\epsilon_2$ with X-ray photoelectron spectra (ESCA), for both the amorphous and orthorhombic crystalline (D_{2h}^{16}) modifications of the same composition. The single crystals were prepared in a horizontal zone-refiner[1] and the amorphous films by vacuum evaporation[2] on to room-temperature fused-quartz or, for ESCA, aluminum substrates. An electrically conducting substrate of aluminum was used to facilitate cleaning by sputtering. The films were verified to be amorphous by X-ray diffraction.

Values for the function $(h\nu)^2\epsilon_2$, where ν is the photon energy, were calculated by Kramers-Kronig analysis[3] of reflectivity data from 0 to 24 eV[4] and are plotted in Fig. 1. The most striking difference between the amorphous and single-crystal curves is that the peak observed at ~3 eV for both polarizations of the electric light vector for the single crystal appears to be strongly depressed for the amorphous material. This peak and the next major one at ~9 eV also are less well resolved for the amorphous solid.

The FSCA data were taken on freshly sputtered single crystal and amorphous specimens. Argon sputtering removed surface impurity photoelectron peaks but did not appear to change the overall shape of the spectra of either the amorphous or single crystal specimens.

In Fig. 2 the X-ray photoelectron energy distribution curves are plotted in the range zero to 45 eV, with the zero of energy at the Fermi-level. The curves for the single crystal and amorphous specimens are in general remarkably similar. A triplet structure appears in the ESCA data for the crystalline samples at about 14 eV. This structure was not resolved as a triplet in the amorphous data. The spectrometer resolution for this measurement was ∿1 eV (full width, half maximum). The strong triplet peak at ∿24 eV which appears for both the amorphous and crystalline samples in the ESCA data and, therefore, in the valence band density of states, we associate with the rising $(h\nu)^2\varepsilon_2$ beyond 20 eV. The doublet at ∿33 eV we associate with the Sb $4d_{3/2,5/2}$ levels. The ratio of intensities should be 2:3, and probably is, since the weaker line is riding on the shoulder of the stronger.

As expected, good correspondence was obtained between the structure for amorphous and single crystal material at higher energies, such as the Se $3d_{3/2,5/2}$ doublet at ∿5[illegible] eV and the Sb $3d_{3/2,5/2}$ doublet at 537 and 528 eV shown in Fig. 3. The oxygen $1s_{1/2}$ level lies in the range of the latter doublet and a small amount of oxygen remaining on the surface of the amorphous sample after sputtering could be detected by the weak shoulder at 532 eV.

Since $(h\nu)^2\varepsilon_2$, the transition strength, is representative of the joint density of electronic states for optical transitions (assuming

constant matrix elements) and since ESCA data portray the structure of the occupied bands[5], in particular, the valence band, we conclude that the peak at ∿9 eV in the $(h\nu)^2\epsilon_2$ data arises from the conduction band because of the absence of any corresponding structure in the ESCA data. This peak is unlikely to arise from non-constant matrix elements since it appears with equal strength in the optical data for both crystalline orientations and amorphous material and thus is insensitive to lack of long-range order.

The major effect of the crystalline to amorphous transition appears to be a general decrease of $(h\nu)^2\epsilon_2$ at the lower energy range coupled with a smearing of most structure. Since the ESCA measurements show no large changes in the structure of the valence band between the crystalline and amorphous material (fine structure of width <1 eV would not be resolved) we conclude that the lower observed values of $(h\nu)^2\epsilon_2$ arise either from a lower conduction band density of states or from a suppression of matrix elements in the amorphous material.

---

†This research was supported by the Advanced Research Projects Agency of the Department of Defense and was monitored by the Army Research Office, Durham, under Contract No. DA-ARO-D-31-124-71-G132.

1. C. Wood, B. Van Pelt and E. Hyland (to be published).

2. R. Mueller and C. Wood, J. Non-Cryst. Solids (in press).

3. R. Afshar, F. M. Mueller and J. C. Shaffer, J. Comp. Phys. (in press).

4. C. Wood, Z. Hurych and J. C. Shaffer Proc. of 4th Intern. Conf. on Amorph. and Liq. Semicond., J. Non-Cryst. Solids (in press). J. C. Shaffer, B. Van Pelt, C. Wood, J. Freeouf, K. Murase and J. W. Osmun (to be published).

5. Y. Baer, P. F. Heden, J. Hedman, M. Klasson, C. Nordling and K. Siegbahn, Physica Scripta 1 56 (1970).

FIGURE CAPTIONS

Figure 1: Energy dependence of the optical transition strength for amorphous and for two orientations of single-crystal Sb_2Se_3 with the electric vector E||a and E||c.

Figure 2: The X-ray photoelectron spectra between zero and 45 eV binding energy for a single crystal and an amorphous sample of Sb_2Se_3. The ordinate scale applies only to the single crystal counting rate. The counting rate for the amorphous sample has been scaled and displaced in order to facilitate comparison.

Figure 3: The X-ray photoelectron spectra for two designated energy regions for a single crystal and an amorphous sample of Sb_2Se_3. As in Figure 2, the ordinate scale applies only to the single crystal data and the data for the amorphous sample has been scaled and displaced to facilitate comparison.

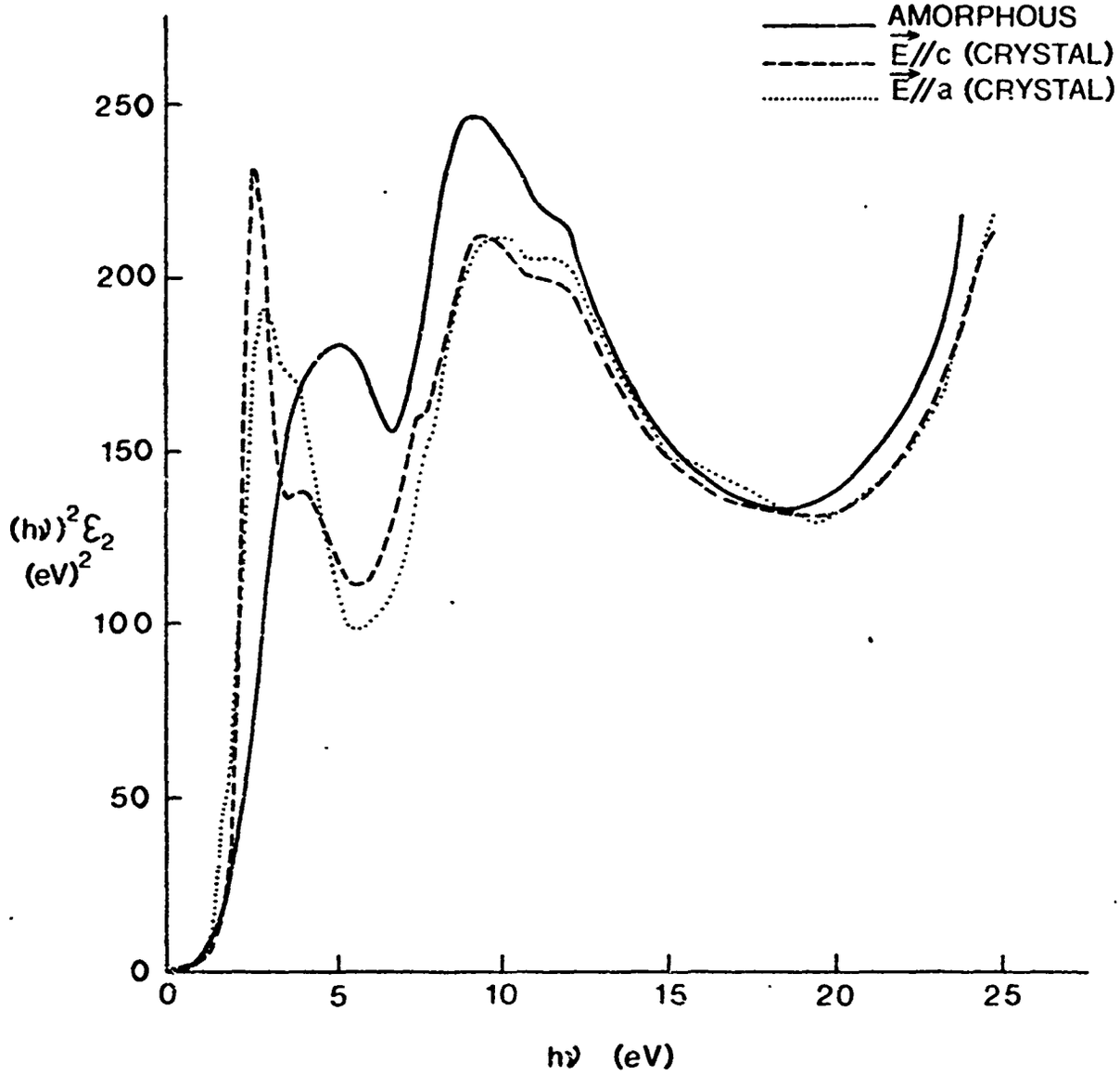
AMORPHOUS
E//c (CRYSTAL)
E//a (CRYSTAL)
250
200
150
100
50
0
$(h\nu)^2\varepsilon_2$
$(eV)^2$
0
5
10
15
20
25
$h\nu$ (eV)

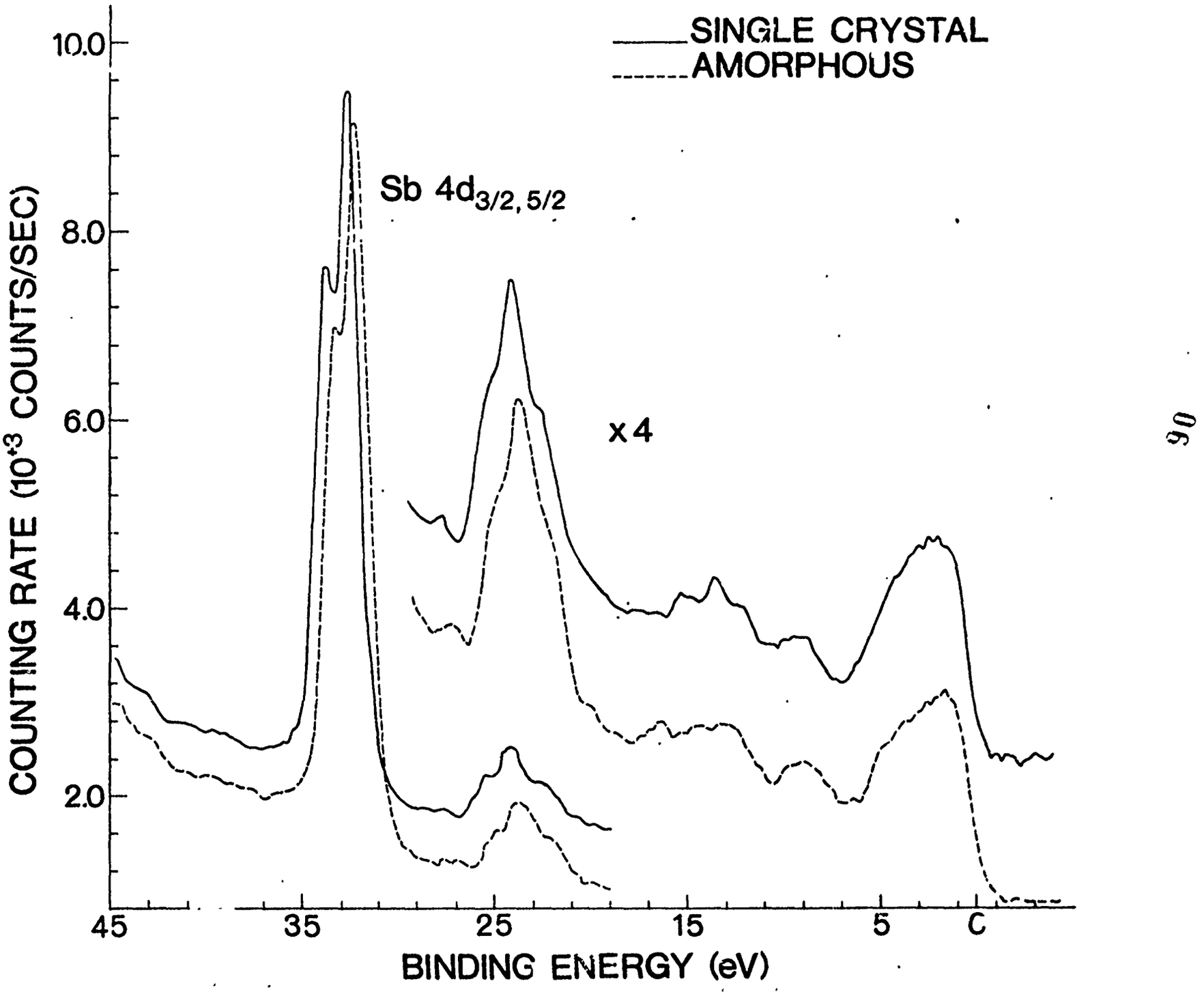
SINGLE CRYSTAL
AMORPHOUS
Sb 4d3/2,5/2
x4
COUNTING RATE (10-3 COUNTS/SEC)
10.0
8.0
6.0
4.0
2.0
45
35
25
15
5
0
BINDING ENERGY (eV)

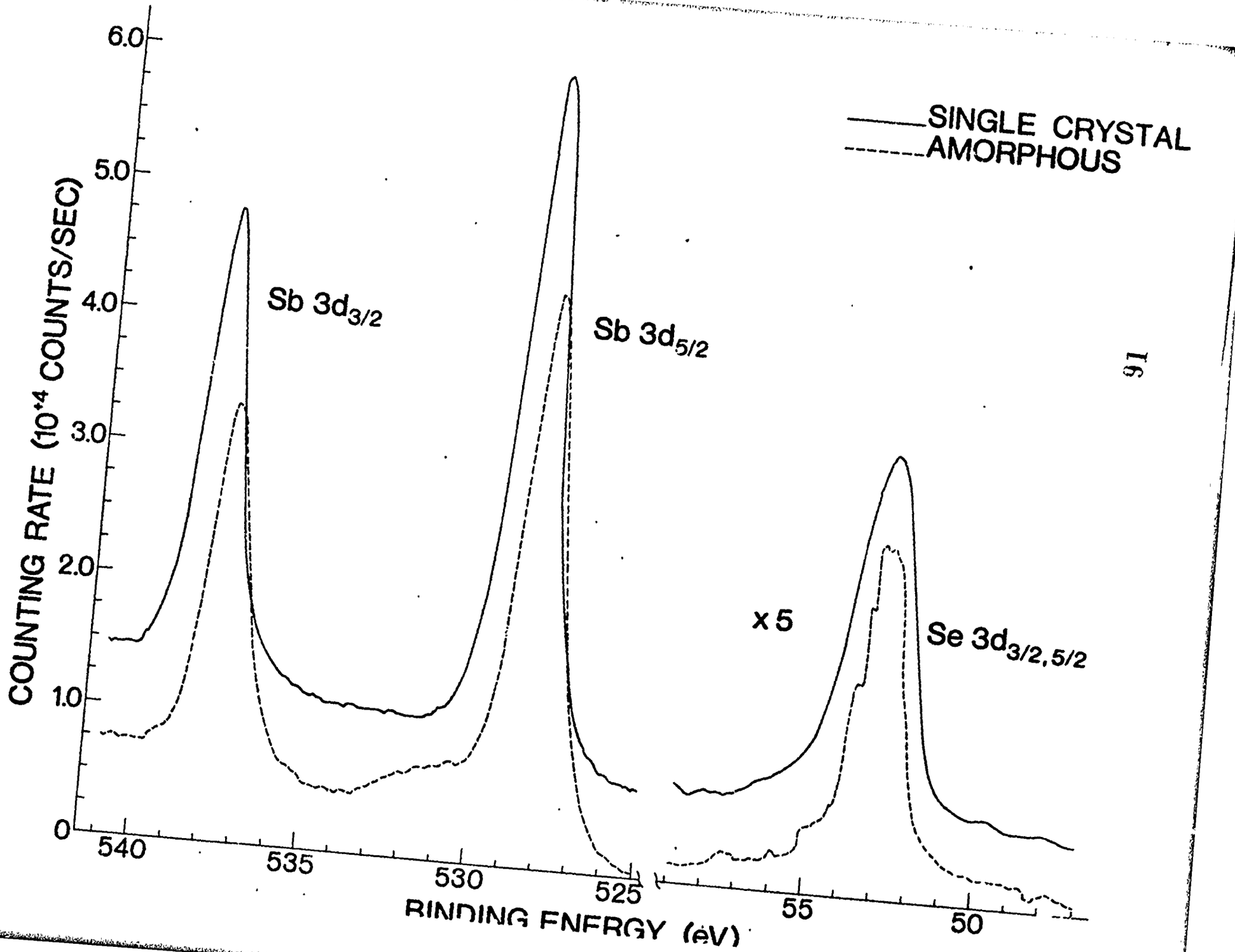
SINGLE CRYSTAL
AMORPHOUS
COUNTING RATE (10^{+4} COUNTS/SEC)
6.0
5.0
4.0
3.0
2.0
1.0
0
Sb $3d_{3/2}$
Sb $3d_{5/2}$
x 5
Se $3d_{3/2,5/2}$
540
535
530
525
55
50
BINDING ENERGY (eV)

APPENDIX D

Amorphous and Crystalline Sb_2O_3†

B. Van Pelt, C. Wood and A. Dwight
Physics Department
Northern Illinois University
DeKalb, Illinois 60115

As part of a study of the homologous series of compounds of Sb with Group VI elements we have investigated the optical properties of antimony oxide Sb_2O_3 in the amorphous and crystalline forms. Sb_2O_3 has two crystalline modifications: orthorhombic Pccn, D_{2h}^{10} and cubic Fd3m, O_h^7. Both forms exist as natural minerals, the former as valentinite and the latter as senarmontite. The homologous compounds Sb_2Se_3 and Sb_2S_3 occur only in the orthorhombic form Pbnm, D_{2h}^{16}.

The crystals were prepared by enclosing a charge of Sb_2O_3 powder in a sealed evacuated quartz tube 40 cm long and placing the tube in a temperature gradient such that the end containing the powder was at 680°C and the other end at room-temperature. Small orthorhombic needles having dimensions of a few mm length and fractions of a mm in cross-section with the growth axis in the c-direction were produced in the region of the tube above 570°C [1]. Triangular-faceted cubic crystals of dimension several mm on a side were formed in the regions just below 570°C. In addition, material deposited on the walls of the tube (or on fused quartz substrates) as an amorphous film was also investigated optically.

The structure and single-crystallinity of each phase was determined by X-ray diffraction. A Debye-Scherrer X-ray diffraction pattern was taken with a copper target on a specimen of cubic Sb_2O_3. The lines of a

face-centered cubic lattice were present, with a_o = 11.152Å, in agreement with the value on ASTM card 5-0534. For the orthorhombic Sb_2O_3, a pattern showed lines which agree with those on ASTM card 11-689, therefore it was assumed that the quoted cell constants were correct: a = 4.914Å, b = 12.468Å, c = 5.421Å. The volumes per formula weight (V/M) were calculated to permit a comparison of packing efficiency giving values of 86.67A^3 (cubic) and 83.03A^3 (orthorhombic), indicating a more efficient packing in the high-temperature orthorhombic form.

Reflectance and transmission measurements were made on all three forms of Sb_2O_3, including E||b and E||c for the orthorhombic structure. Data analysis, in the short-wavelength spectral region where there were no interference fringes was performed by computer programming the method of Nazarewicz et. al. [2] to determine the refractive index, n and the absorption coefficient α (Fig. 1 and 2). The short-wavelength limit on the measured spectral range was set by the slit width of the Cary 14R spectrophotometer reaching the fully-open position. The absorption edge of the amorphous form was found to obey an approximate $(\alpha h\nu)^{\frac{1}{2}}$ dependence on photon energy ($h\nu$) showing conservation of energy but not crystal momentum [3]. Similarly an $(\alpha h\nu)^{\frac{1}{2}}$ dependence on photon energy was obtained for both single crystal forms of Sb_2O_3 showing that an indirect transition is responsible for the lower part of the absorption edge, as observed for orthorhombic Sb_2S_3 [4] and orthorhombic Sb_2Se_3 [5]. Indirect gaps of $\sim$3.24 eV for E||b, $\sim$3.28 eV for E||c for orthorhombic and 4.0 eV for cubic form were obtained from the intercepts compared with a value of 3.8 eV for the intercept of the amorphous phase (Fig. 3).

Thus it is seen that the optical properties in the vicinity of the energy gap of Sb_2O_3 conform to other members of the homologous series. However, the large shift of the energy gap to higher energies on the orthorhombic crystalline to amorphous transformation is in strong contrast with Sb_2Se_3 in which the indirect edge of the crystalline orthorhombic phase and the edge in the amorphous phase coincide [6].

There appears to be no rule as to which way the energy gap should shift on loss of long-range order. Energy gaps may shift to higher energies (Se, Te [7]) remain the same (Ge [8] Sb_2Se_3 [6]) or shift to lower energy (As_2Se_3, As_2S_3 [9]) at the crystalline to amorphous transformation. Part of the problem lies in the uncertainty as to which region of the absorption edges in the two phases should be compared. Certainly one would expect the most weakly bonded (second, third, etc. nearest-neighbor) atoms and, therefore, the indirect transitions to be most strongly affected by structural randomization. For a more definitive grasp of the effects of randomization on the electronic structure the whole spectrum including direct transitions should be compared. We are currently attempting to grow larger crystals of Sb_2O_3 to obtain more accurate optical data at higher photon energies.

These results, however, suggest that the short-range order in amorphous Sb_2O_3 approximates more closely to that of the cubic form, a conclusion somewhat supported by the Mossbauer studies of Long et. al. [10] where the quadrapole spitting in the amorphous phase more closely corresponds to that of the cubic structure.

ACKNOWLEDGEMENT

We are indebted to L. R. Gilbert for assistance with the computer programming of the optical data.

---

† This work was supported by the Advanced Research Projects Agency of the Department of Defense and was monitored by the Army Research Office, Durham, under Contract No. DA-ARO-D-31-124-71-G132.

1. W. B. Pearson, Handbook of Lattice Spacings and Structures of Metals (Pergamon, 1958).

2. W. Nazarewicz, P. Rolland, E. da Silva and M. Balkauski, Applied Optics 1, 369 (1962).

3. J. Tauc, R. Grigorovici and A. Vancu, Phys. Stat. Sol. 15 627 (1966).

4. A. Audzijonis, J. Batarunas, A. Karpas and Th. Kudrhmanskas, Lietuvos Fizikos Rinkinys, 5 IV, 481 (1965).

5. V. V. Sobolov, S. D. Shutov and S. N. Shesta.:kii, Moldavian Academy of Sciences, U.S.S.R., 183 (1969).

6. C. Wood, Z. Hurych and J. C. Shaffer, Proc. 4th Int. Conf. on Amorphous and Liquid Semicond., J. Non-Cryst Solids (in press).

7. J. Stuke, Translation of talk presented at the German Physical Society Meeting, Munich, March (1969).

8. T. M. Donovan, E. J. Ashley and W. E. Spicer, Phys. Letters 32A 85 (1970).

9. R. Zallen, R. E. Drews, R. L. Emerald and M. L. Slade, Phys. Rev. Letters 26 1564 (1971).

10. G. G. Long, J. G. Stevens and L. H. Bowen, Inorg. Nucl. Chem. Letters 5 799 (1969).

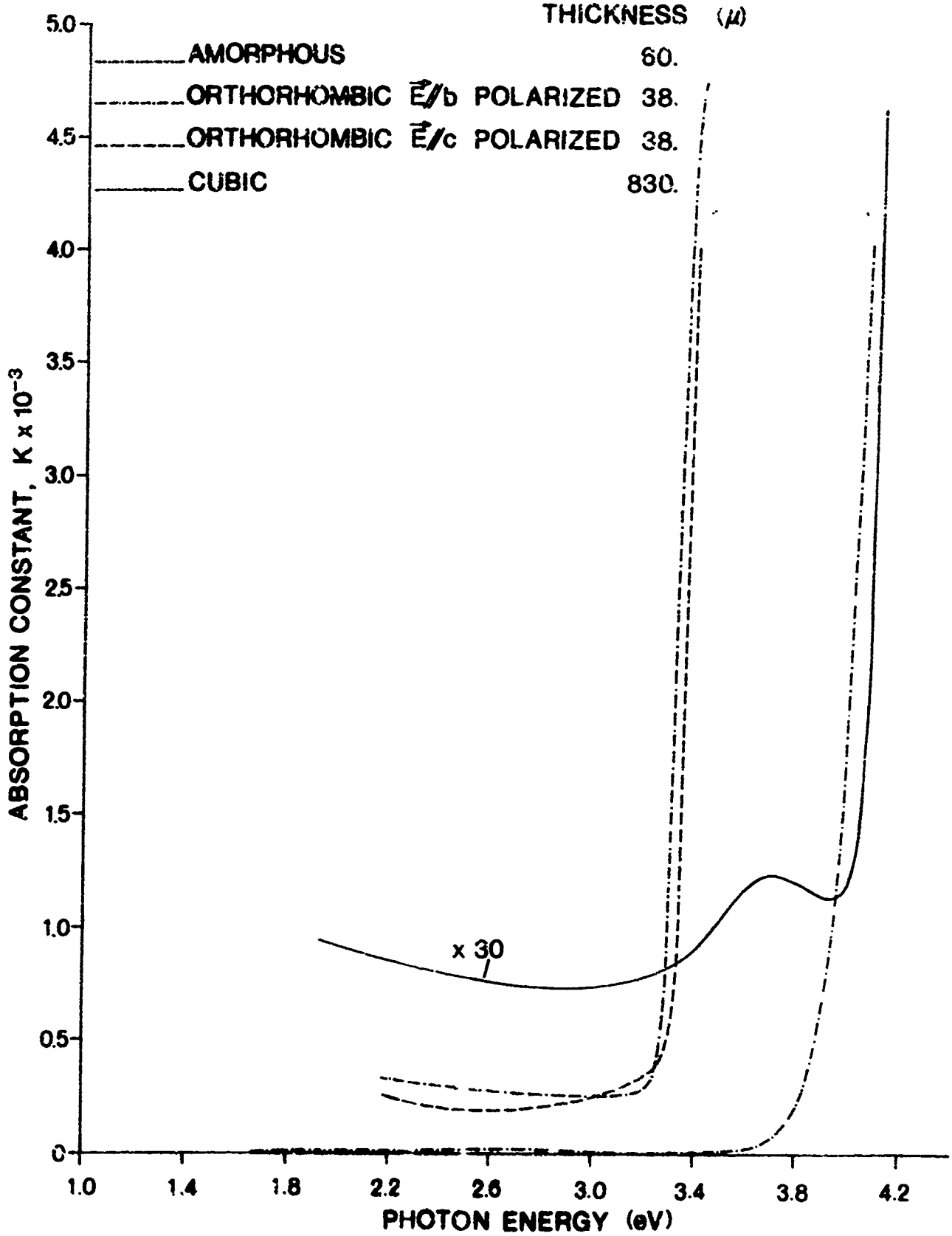
THICKNESS (μ)
AMORPHOUS 60.
ORTHORHOMBIC E//b POLARIZED 38.
ORTHORHOMBIC E//c POLARIZED 38.
CUBIC 830.
x 30
ABSORPTION CONSTANT, K x 10⁻³
PHOTON ENERGY (eV)
5.0
4.5
4.0
3.5
3.0
2.5
2.0
1.5
1.0
0.5
0
1.0
1.4
1.8
2.2
2.6
3.0
3.4
3.8
4.2

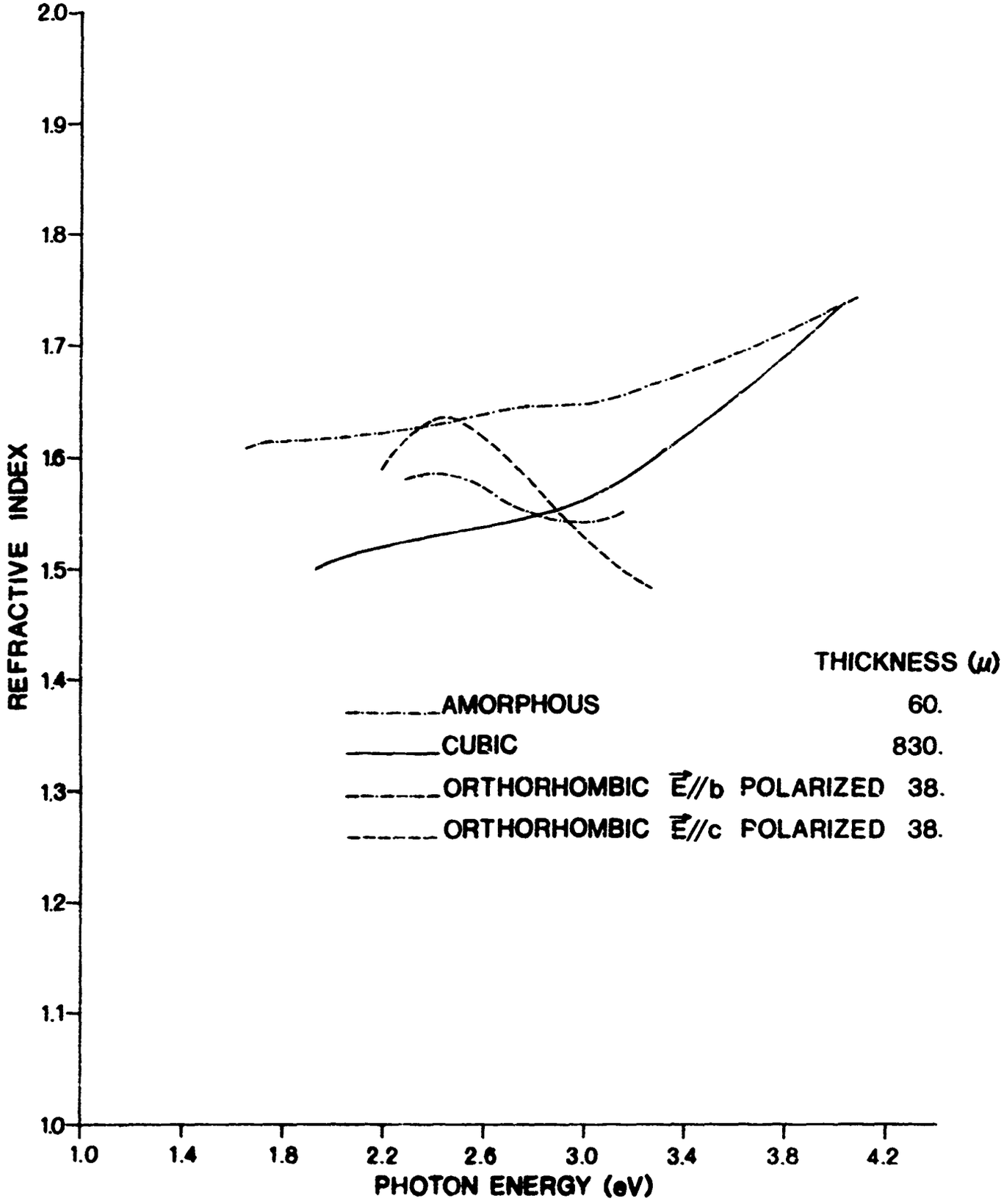
2.0
1.9
1.8
1.7
1.6
1.5
1.4
1.3
1.2
1.1
1.0
REFRACTIVE INDEX
1.0
1.4
1.8
2.2
2.6
3.0
3.4
3.8
4.2
PHOTON ENERGY (eV)
THICKNESS (μ)
AMORPHOUS 60.
CUBIC 830.
ORTHORHOMBIC E//b POLARIZED 38.
ORTHORHOMBIC E//c POLARIZED 38.

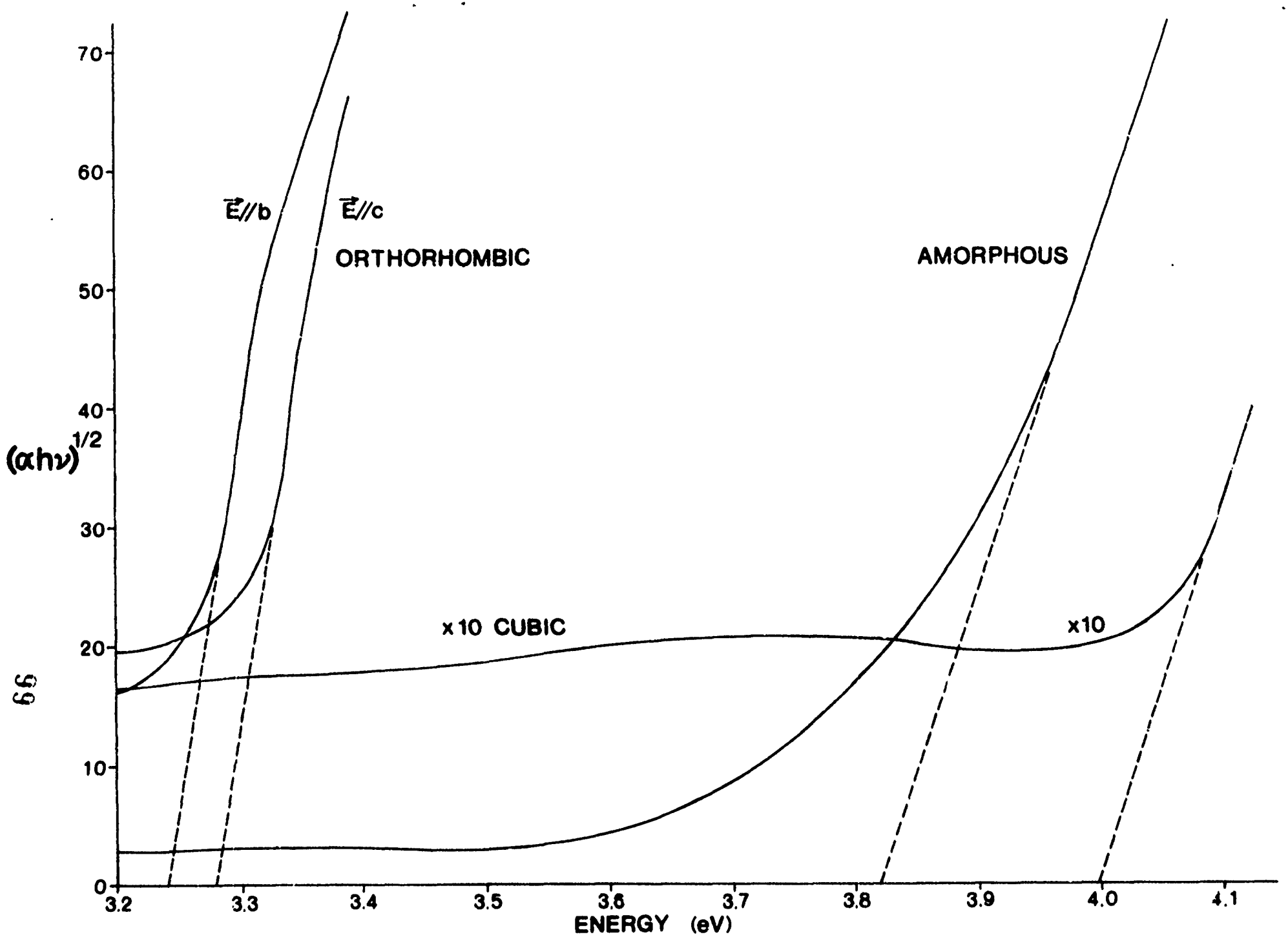
70
60
50
40
30
20
10
0
$(\alpha h\nu)^{1/2}$
$\vec{E}//b$
$\vec{E}//c$
ORTHORHOMBIC
AMORPHOUS
x10 CUBIC
x10
3.2
3.3
3.4
3.5
3.6
3.7
3.8
3.9
4.0
4.1
ENERGY (eV)

APPENDIX E

Abstract Submitted

for the 1972 March Meeting of the

American Physical Society

27-30 March 1972
Date

Physical Review
Analytic Subject Index
Number 44.4

Bulletin Subject Heading
in which Paper should be placed

Semiconductors - Optical Properites

Optical Functions of Amorphous Thin Films From Reflectivity and Transmission Data by an Approximate Quadratic Inversion* J. C. SHAFFER and L. R. GILBERT, Northern Illinois Univ.--In this paper we present a computational technique to obtain the optical functions of thin films upon substrates directly from nearly exact inversion of the equations for the reflectance and transmittance of a stratified medium. The method, which is a local quadratic interpolation procedure, is designed to exploit the continuity of the complex refractive index in wavelength in order to avoid the pitfalls associated with the non-uniqueness of the inversion of the exact equations. The method is applied to data generated from classical dispersion theory as well as to data measured upon thin amorphous films of Se and Sb_2Se_3. The optical functions of these materials as obtained by this method are discussed and compared with previous results.

*Supported by A.R.P.A. through A.R.C., Durham.

Submitted by
John C. Shaffer
Signature of APS Member

John C. Shaffer
Same name typewritten

Department of Physics, NIU
Address

DeKalb, Illinois 60115

Abstract Submitted

for the 1972 March Meeting of the

American Physical Society

27-30 March 1972

Physical Review
Analytic Subject Index
Number
48.3

Bulletin Subject Heading
in which Paper should be placed

Amorphous Solids

Amorphous and Crystalline Sb_2O_3.* B. VAN PELT and C. WOOD, Northern Illinois University--The optical properties of amorphous thin films of Sb_2O_3 and single-crystal platelets of orthorhombic Sb_2O_3 have been compared in the vicinity of the band gap at ~3.3 eV. Both forms were prepared by vacuum evaporation in a closed system. As in the homologous compounds Sb_2S_3 and Sb_2Se_3 the absorption edge in the crystalline material is found to begin with an indirect transition. The edge in the amorphous modification has a similar energy dependence suggesting the optical transitions conserve energy but not crystal momentum.[1]

*Supported by A.R.P.A. through A.R.O., Durham.

[1]J. Tauc, R. Grigorovici and A. Vancu, Phys. Stat. Sol. 15, 627 (1966).

Submitted by

Signature of APS Member

Charles Wood
Same name typewritten

Department of Physics, NIU
Address
DeKalb, Illinois 60115

Abstract Submitted
For the March Meeting of
The American Physical Society
27-30 March, 1972

Physical Review
Analytic Subject Index
Number 44.3

Bulletin Subject Heading in which Paper should be placed
Amorphous Semiconductors

Reflectance Spectra of Several Chalcogenide Semiconductors.* K.MURASE, J.W.OSMUN, J.FREEOUF and MARC KASTNER,† The University of Chicago and C.WOOD, Northern Illinois University -- Near normal incidence reflectivity was measured for a-As_2S_3, a-$GeSe_2$, an alloy glass $Ge_{16}As_{35}Te_{28}S_{21}$ and a- and c-Sb_2Se_3 (a=amorphous, c=crystalline). Synchrotron radiation from the University of Wisconsin electron storage ring was used in the energy range 4-30 eV. Well defined broad peaks appeared near 3-5 eV, 8-10 eV and 12-13 eV for all these materials. For c-Sb_2Se_3, strong anisotropy was observed in the region $h\nu < 4$ eV. The high energy spectra are similar for c- and a-Sb_2Se_3. An attempt is made to interpret the three broad peaks in the spirit of the chemical bond model.[1] The low energy peak then represents transitions between nonbonding and antibonding states. The higher peaks are either due to bonding-antibonding transitions or transitions between s states and antibonding states.

*Work supported by AFOSR and carried out at the University of Wisconsin Physical Science Laboratory.
†Hertz Foundation Fellow.
[1]E.Mooser and W.B.Pearson, in Progress in Semiconductors 5, 104 (1960).

Submitted by

Marc Kastner
James Franck Institute
The University of Chicago
5640 S. Ellis Avenue
Chicago, Illinois 60637